This peer-reviewed published paper appears as: Akcelyan, S., Lignos, D. G. and Hikino, T. (2018). "Adaptive Numerical Method Algorithms for Nonlinear Viscous and Bilinear Oil Damper Models Subjected to Dynamic Loading". Soil Dynamics and Earthquake Engineering, Vol. 113, pp. 488-502. DOI: 10.1016/j.soildyn.2018.06.021

Adaptive Numerical Method Algorithms for Nonlinear Viscous and Bilinear Oil Damper Models Subjected to Dynamic Loading

Sarven Akcelyan[a], Dimitrios G. Lignos[b], Tsuyoshi Hikino[c]

ABSTRACT

Adaptive numerical method algorithms are presented for the numerical simulation of the hysteretic behavior of nonlinear viscous and bilinear oil dampers within a finite element program for nonlinear dynamic analysis of frame structures under earthquake excitations. The adaptive algorithms are applicable for computing high-precision solutions for nonlinear viscous and bilinear oil dampers with valve relief that are typically represented mathematically with a nonlinear Maxwell model. The algorithms presented possess excellent convergence characteristics for viscous dampers with a wide range of velocity exponents and axial stiffness properties. The algorithms are implemented in an open source finite element software, and their applicability and computational efficiency is demonstrated through a number of validation examples with data that involve component experimentation as well as the utilization of full-scale shake table tests of a 5-story steel building equipped with nonlinear viscous and bilinear oil dampers.

Keywords: nonlinear viscous damper; bilinear oil damper; fluid viscous damper; supplemental damping; passive control; response modification; numerical simulation; full-scale shake table test.

---

[a]Ph.D., Course Lecturer, Dept. of Civil Engineering and Applied Mechanics, McGill University, Montreal, QC, H3A 2K6

[b]Associate Professor, Dept. of Architecture, Civil and Environmental Engineering, Ecole Polytechnique Fédérale de Lausanne (EPFL), EPFL ENAC IIC RESSLab, GC B3 485, Station 18, CH-1015 Lausanne, Switzerland

[c]Ph.D., Section Manager, Building Construction & Steel Structures Division, Nippon Steel and Sumikin Engineering Co., Ltd, Tokyo, Japan, Former Researcher, E-Defense, National Research Institute for Earth Science and Disaster Prevention (NIED)

1. Introduction

In the past three decades various types of supplemental damping devices have been developed and utilized in frame buildings to control seismic and wind-induced vibrations (Constantinou and Symans

This peer-reviewed published paper appears as: Akcelyan, S., Lignos, D. G. and Hikino, T. (2018). "Adaptive Numerical Method Algorithms for Nonlinear Viscous and Bilinear Oil Damper Models Subjected to Dynamic Loading". Soil Dynamics and Earthquake Engineering, Vol. 113, pp. 488-502. DOI: 10.1016/j.soildyn.2018.06.021

1993; Soong and Dargush 1997; Christopoulos and Filiatrault 2006; Black and Makris 2007; Symans et al. 2008; Dong et al. 2015). To this end, viscous dampers are advantageous as the forces they develop are typically out-of-phase with displacement-induced forces within a frame building under earthquake loading (Constantinou et al. 1998). Recent earthquakes demonstrated the effectiveness of viscous dampers in response modification of conventional buildings to control structural and non-structural damage (Buchanan et al. 2011; Miranda et al. 2012; Kasai et al. 2013).

For the successful implementation of viscous dampers into the earthquake engineering design practice the availability of mathematical models that represent accurately the hysteretic response of such devices is necessary. Rigorous integration methods are essential for the numerical solution of these models when nonlinear response history analysis (NRHA) is conducted. Unlike in solid viscoelastic dampers (Chang et al. 1995) the temperature dependency of fluid viscous dampers is relatively low (Kasai et al. 2004b; Symans et al. 2008). In contrast with the idealized assumption of purely viscous dashpot models, viscous dampers show stiffness dependency characteristics that generally undermine the effectiveness of a viscous damper (Makris and Constantinou 1991). Although a number of researchers, have studied the effect of axial stiffness of viscous dampers on the seismic performance of frame buildings (Constantinou et al. 2001; Singh et al. 2003; Chen and Chai 2011; Liang et al. 2011; Londoño et al. 2013), they mainly focused on linear viscous dampers. In the case of nonlinear viscous dampers, a common practice has been to neglect the damper axial stiffness (Pekcan et al. 1999; Ramirez et al. 2001; Lin and Chopra 2002; Hwang et al. 2008; Diotallevi et al. 2012). This is a convenient assumption because a closed-form analytical solution of the damper force can be computed when NRHA is employed. Recent shake table experiments of a full-scale 5-story steel frame building equipped with viscous dampers that were conducted at the world's largest shake table around the world (Ooki et al. 2009; Kasai and Matsuda 2014) demonstrated that the consideration of the damper axial stiffness is critical in order to accurately predict both local and global seismic demands of the test structure (Kasai et al. 2007; Kasai and Matsuda 2014).

This peer-reviewed published paper appears as: Akcelyan, S., Lignos, D. G. and Hikino, T. (2018). "Adaptive Numerical Method Algorithms for Nonlinear Viscous and Bilinear Oil Damper Models Subjected to Dynamic Loading". Soil Dynamics and Earthquake Engineering, Vol. 113, pp. 488-502. DOI: 10.1016/j.soildyn.2018.06.021

A blind analysis contest that was conducted to challenge the existing modeling capabilities for steel frame buildings equipped with various types of dampers demonstrated that when the brace and damper axial stiffness is incorporated in nonlinear viscous dampers, it improves the overall prediction accuracy by more than 20% compared to the experimental data (Yu et al. 2013). Recent studies (Dong et al. 2015, 2018) have shown that the displacement-induced forces and damper force demands may be in phase within a frame building due to the axial stiffness of the respective damper. This has a profound effect on the seismic demands transferred to the steel columns and foundations and should be carefully quantified. Several researchers have proposed ways to account for the stiffening and frequency dependency of viscous dampers and to compute numerically their hysteretic response under harmonic and seismic excitations by employing the Maxwell model (Makris and Constantinou 1991; Constantinou and Symans 1993; Reinhorn et al. 1995; Takahashi and Sekiguchi 2001; Oohara and Kasai 2002; Singh et al. 2003). Typical fixed time-step integration algorithms that have been employed to obtain numerically the viscous damper hysteretic response may require considerably small integration steps to overcome convergence problems (Oohara and Kasai 2002). In particular, numerical convergence may still be a challenge for frame buildings equipped with nonlinear viscous dampers with high axial stiffness and small velocity exponents (Oohara and Kasai 2002). In such cases, a smaller integration time step for the overall analysis is necessary. This reduces the computational efficiency of the analysis of building models with nonlinear viscous dampers. This may also be a fundamental constraint for the optimal seismic design and/or retrofit of frame buildings with nonlinear viscous dampers in which the locations as well as the damper sizes should be explicitly identified as part of the optimization problem (Lavan et al. 2008; Lavan and Avishur 2013; Pollini et al. 2017). It is understood that improved integration algorithms should be utilized to reliably obtain the numerical solution of nonlinear viscous damper models.

Others have proposed ways to account for the stiffening and frequency dependency of viscous dampers to compute their hysteretic response under harmonic and seismic excitations. For

This peer-reviewed published paper appears as: Akcelyan, S., Lignos, D. G. and Hikino, T. (2018). "Adaptive Numerical Method Algorithms for Nonlinear Viscous and Bilinear Oil Damper Models Subjected to Dynamic Loading". Soil Dynamics and Earthquake Engineering, Vol. 113, pp. 488-502. DOI: 10.1016/j.soildyn.2018.06.021

instance, Terenzi (1999) has employed the Kelvin-Voigt model, in which *a* spring is connected parallel to a dashpot. This modeling approach is commonly utilized for solid viscoelastic devices. However, a Maxwell model (i.e., spring connected in series with a dashpot), has been found to be more appropriate to account for both the stiffness and frequency dependency of fluid viscoelastic dampers (Makris and Constantinou 1991; Constantinou and Symans 1993; Reinhorn et al. 1995; Takahashi and Sekiguchi 2001; Oohara and Kasai 2002; Singh et al. 2003). Others (Sivaselvan et al. 2009) have utilized a mixed Lagrangian approach to conduct nonlinear response history analyses of frame structures with linear and nonlinear viscous dampers.

This paper discusses the numerical implementation of an improved adaptive algorithm for the numerical solution of the constitutive equations of nonlinear viscous and bilinear oil damper material models under dynamic loading when the axial stiffness of the dampers is considered as part of the constitutive damper formulation. The efficiency of the proposed algorithms is compared with that of traditional integration schemes that are typically used for the numerical solution of initial value problems. The proposed numerical solution techniques are implemented in an open-source finite element simulation platform and are validated with full-scale tests from nonlinear viscous and bilinear oil dampers subjected to sinusoidal excitations and various loading frequencies. Furthermore, experimental data from a 5-story steel building with the same damper types that was tested at full-scale is utilized to demonstrate the efficiency of the proposed adaptive numerical schemes in predicting global and local engineering demand parameters of frame buildings equipped with supplemental damping devices. Finally, the paper provides tools to aid the preliminary design of steel frame buildings equipped with nonlinear viscous dampers so as analysis iterations with unnecessarily too stiff or too flexible damper models can be eliminated.

This peer-reviewed published paper appears as: Akcelyan, S., Lignos, D. G. and Hikino, T. (2018). "Adaptive Numerical Method Algorithms for Nonlinear Viscous and Bilinear Oil Damper Models Subjected to Dynamic Loading". Soil Dynamics and Earthquake Engineering, Vol. 113, pp. 488-502. DOI: 10.1016/j.soildyn.2018.06.021

2. Hysteretic Behaviour of Viscous Dampers as Pure Viscous Models

Viscous dampers contain a polymer liquid and its flow through orifices leads to pressure differential across a piston head, which produces the damper force. The design of orifice dictates the relationship between the force and velocity. Thus, the general force-velocity relationship of nonlinear viscous models can be mathematically expressed by Equation (1) (Symans and Constantinou 1998),

$$F_d(t) = C_d \left|\dot{u}_d(t)\right|^{\alpha} \operatorname{sgn}\left(\dot{u}_d(t)\right) \tag{1}$$

in which, C_d is the damping coefficient and α is the velocity exponent that characterizes the viscous material; u_d is the dashpot displacement ; and sgn represents the signum function. Thus, the peak force F_{d0} of a viscous damper under a harmonic displacement excitation that is described as $u_d(t) = u_{d0}\sin(\omega t)$, is as follows,

$$F_{d0} = C_d(\omega u_{d0})^{\alpha} \tag{2}$$

in which, u_{d0} and ω are the peak displacement amplitude and the circular frequency of the sinusoidal excitation, respectively. Figure 1 shows the normalized force-velocity and normalized force-displacement relations of nonlinear viscous models with different α values. A typical Bernoullian cylindrical shaped orifice produces forces, which are proportional to the square of the velocity (i.e., $\alpha = 2$). Such dampers are utilized for shock wave absorption. For $\alpha = 1$, a viscous damper becomes linear while for $\alpha = 0$ the force-displacement hysteretic relation of a viscous damper becomes rectangular, which is typical for friction models (Pall and Marsh 1982). For seismic design applications of frame buildings the capability of limiting the damper force output under high velocity pulses is often desirable. Therefore for seismic applications, α is often selected such that $\alpha < 1$. Because linear viscous dampers produce forces that vary linearly with respect to the velocity demand, large damper forces may be generated under high velocity demands. This introduces uncertainties and conservatism in capacity design of non-dissipative members. In order to overcome this undesirable response, bilinear oil dampers were developed that contain a relief

This peer-reviewed published paper appears as: Akcelyan, S., Lignos, D. G. and Hikino, T. (2018). "Adaptive Numerical Method Algorithms for Nonlinear Viscous and Bilinear Oil Damper Models Subjected to Dynamic Loading". Soil Dynamics and Earthquake Engineering, Vol. 113, pp. 488-502. DOI: 10.1016/j.soildyn.2018.06.021

mechanism, which suppresses the force after a certain limit (Ichihasi et al. 2000; Kasai and Nishimura 2004; Kasai et al. 2004b; Tsuyuki et al. 2004). This creates a bilinear relation between the damper force and velocity as shown in Figure 2a. Thus, the force produced by a bilinear oil damper can be computed as follows,

$$F_d(t) = \begin{cases} C_d \dot{u}_d(t), & |F_d(t)| \le F_{dr} \\ \operatorname{sgn}\left(\dot{u}_d(t)\right)\left(F_{dr} + pC_d\left(|\dot{u}_d(t)| - \dot{u}_{dr}\right)\right), & |F_d(t)| > F_{dr} \end{cases} \quad (3)$$

in which, p is the post relief damping coefficient ratio; F_{dr} and $\dot{u}_{dr}$ are the relief force and relief velocity of the bilinear oil damper, respectively. The peak force F_{d0} of a bilinear oil damper under sinusoidal displacement excitation $u_d(t) = u_{d0}\sin(\omega t)$ can be computed as follows,

$$F_{d0} = \left(p + \frac{1-p}{\mu_d}\right) C_d \omega u_{d0} \quad (4)$$

the peak damper velocity ratio, μ_d of a bilinear oil damper, which is defined as the ratio of maximum velocity demand over the damper relief velocity can be computed as follows,

$$\mu_d = \frac{\dot{u}_{d0}}{\dot{u}_{dr}} = \frac{\omega u_{d0}}{\dot{u}_{dr}} \quad (5)$$

Figure 2b illustrates the hysteretic behaviour of a bilinear oil damper under sinusoidal loading for different displacement amplitudes. In this figure, the horizontal axis has been normalized with respect to the peak displacement amplitude. The damper was designed for a peak damper velocity, $\mu_d = 3$. The post-relief damping coefficient ratio was assumed to be $p = 0.1$. The displacement amplitudes were increased in three steps. During the first step, the peak damper velocity was nearly equal to the damper relief velocity; therefore the hysteretic behaviour of the damper was identical to that of a linear viscous damper (Kasai et al. 2004b; Tsuyuki et al. 2004). Once the velocity demand exceeds the damper relief velocity, the relief mechanism is activated and the damping coefficient, C_d, suddenly drops as shown in Figure 2a.

This peer-reviewed published paper appears as: Akcelyan, S., Lignos, D. G. and Hikino, T. (2018). "Adaptive Numerical Method Algorithms for Nonlinear Viscous and Bilinear Oil Damper Models Subjected to Dynamic Loading". Soil Dynamics and Earthquake Engineering, Vol. 113, pp. 488-502. DOI: 10.1016/j.soildyn.2018.06.021

3. Hysteretic Behaviour of Viscous Dampers as Maxwell Models

Prior experimental findings suggest that the hysteretic behaviour of a viscous damper is dependent on its axial internal stiffness K_d, as well as the frequency characteristics of the external applied force (Constantinou and Symans 1993). Typically, K_d can be obtained empirically from experimental data as discussed in Makris and Constantinou (1991) and Kasai et al. (2004a; 2004b). Referring to Figure 3a, viscous dampers in frame buildings are typically installed with supporting braces that consist of several components (e.g., steel braces, clevises, brackets and gusset plates). These components provide additional axial flexibility to the damper and affect its hysteretic behaviour under dynamic loading. The axial flexibility of a viscous damper can be further decomposed into its various components as shown schematically in Figure 3b. In this figure, K_b, K_{cl}, K_{gus} are the stiffness contributions of the steel brace, clevis-brackets and gusset plates, respectively. The gap due to the fabrication tolerance of the damper clevis is noted as G_{cl} in the same figure. To this end, the Maxwell model (Maxwell 1867) has been found to represent well both the axial stiffness and frequency dependency of a viscous damper under dynamic loading (Makris and Constantinou 1991; Constantinou and Symans 1993; Singh et al. 2003). In this case, a nonlinear dashpot and a linear spring are connected in series as illustrated in Figure 3c. The axial stiffness of the damper portion, K_d, and that of the various supporting components (see Figure 3b) can be represented by an equivalent axial stiffness, K_s, as follows,

$$\frac{1}{K_s} = \frac{1}{K_d} + \frac{1}{K_b} + \frac{2}{K_{cl}} + \frac{2}{K_{gus}} \tag{6}$$

The force, F_d at the nonlinear dashpot and spring (F_s) are equal; therefore, the constitutive rules within a Maxwell model can be written as follows,

$$F_d(t) = F_s(t) = K_s u_s(t) \tag{7}$$

$$u_m(t) = u_s(t) + u_d(t) \tag{8}$$

$$\acute{u}_m(t) = \acute{u}_s(t) + \acute{u}_d(t) \tag{9}$$

This peer-reviewed published paper appears as: Akcelyan, S., Lignos, D. G. and Hikino, T. (2018). "Adaptive Numerical Method Algorithms for Nonlinear Viscous and Bilinear Oil Damper Models Subjected to Dynamic Loading". Soil Dynamics and Earthquake Engineering, Vol. 113, pp. 488-502. DOI: 10.1016/j.soildyn.2018.06.021

168 in which, u_m, u_d and u_s are the total, dashpot and spring displacements, respectively (see Figure 3c). The
169 constitutive equation that describes the force and total velocity relation within a Maxwell model can be
170 obtained if Equations (7) and (8) are substituted into Equation (9). For a nonlinear viscous damper this
171 equation is as follows,

172 $$F_d'(t) = \left(\acute{u}_m(t) - \text{sgn}(F_d(t)) \left(\frac{|F_d(t)|}{C_d} \right)^{1/\alpha} \right) K_s, \quad F_d(t_0) = F_0 \tag{10}$$

173 in which, F_0 is damper force at time t_0. For a bilinear oil damper, the following equations hold true,

174 $$F_d'(t) = \begin{cases} \left(\acute{u}_m(t) - \dfrac{F_d(t)}{C_d} \right) K_s, & |F_d(t)| \le F_{dr} \\ \left(\acute{u}_m(t) - \dfrac{\text{sgn}(F_d(t))(p-1)F_{dr} + F_d(t)}{pC_d} \right) K_s, & |F_d(t)| > F_{dr} \end{cases}, \quad F_d(t_0) = F_0 \tag{11}$$

175 Equations (10) and (11) are first order ordinary differential equations that can only be solved numerically
176 in the case of a random vibration input loading.

177

178 **4. Numerical Solution for Nonlinear Viscous and Bilinear Oil Dampers**

179 This section discusses a numerical solution scheme for Equations (10) and (11). For this reason, both
180 equations are treated as a general initial value problem that is described by Equation (12) as follows,

181 $$y' = f(t_n, y_n), \quad y(t_0) = y_0, \tag{12}$$

182 Oohara and Kasai (2002) implemented the classical 4th order Runge-Kutta (RK4) explicit iterative method
183 (Kutta 1901; Butcher 1996) to solve Equation (12) for nonlinear viscous dampers. They stated that the
184 classical RK4 method requires very small integration time steps, h, for large K_s values. For NRHA of
185 frame buildings under earthquake excitations, the maximum value of h is limited by the overall analysis
186 time step dt_a of the integration algorithm that is employed for the numerical solution of the equation of
187 motion; while dt_a should be selected at most equal to the time step of the input ground motion dt

This peer-reviewed published paper appears as: Akcelyan, S., Lignos, D. G. and Hikino, T. (2018). "Adaptive Numerical Method Algorithms for Nonlinear Viscous and Bilinear Oil Damper Models Subjected to Dynamic Loading". Soil Dynamics and Earthquake Engineering, Vol. 113, pp. 488-502. DOI: 10.1016/j.soildyn.2018.06.021

188 depending on the selected integration algorithm to conduct the NRHA; the ratio of dt/dt_a should be an
189 integer. Typical sampling time steps of recorded ground motions vary between 0.005-0.02 sec. However,
190 for a large axial damper stiffness, K_s a much smaller step h should be considered for the utilization of the
191 RK4 iterative method and subsequently the overall NRHA time step dt_a should be further decreased. This
192 could be computationally expensive particularly in 3-dimensional nonlinear response history analysis of
193 frame structures.

194 Alternatively, adaptive solution algorithms may be used. In this section, we utilize the Dormand-Prince
195 (DP54) explicit iterative method (Dormand and Prince 1980) as the basis to solve numerically Equation
196 (12). The solution of this equation is tested with the absolute error predicted between 4th and 5th order
197 solutions. The 4th order solution and the associated absolute error according to the DP54 iterative method
198 for Equation (12) are computed based on Equations (13) and (14), respectively, as follows,

199
$$y_{n+1} = y_n + \frac{35}{384}k_1 + \frac{500}{1113}k_3 + \frac{125}{192}k_4 - \frac{2187}{6784}k_5 + \frac{11}{84}k_6 \tag{13}$$

200
$$\varepsilon_{n+1} = \left| \frac{71}{57600}k_1 - \frac{71}{16695}k_3 + \frac{71}{1920}k_4 - \frac{17253}{339200}k_5 + \frac{22}{525}k_6 - \frac{1}{40}k_7 \right| \tag{14}$$

201 in which y_{n+1} and y_n are the solutions for Equation (12) for the current and previous steps, respectively;
202 ε_{n+1} is the absolute error of the numerical solution in the current step. Note that the term k_2 should not
203 appear in Equations (13) and (14) as summarized in Hairer et al. (1993). From Equations (15) to (21), the
204 DP54 explicit iterative method uses six function evaluations in order to calculate the 4th and 5th order
205 accurate numerical solutions for Equation (14). These function evaluations are computed as follows,

206
$$k_1 = hf(t_n, y_n) \tag{15}$$

207
$$k_2 = hf\left(t_n + \frac{1}{5}h, y_n + \frac{1}{5}k_1\right) \tag{16}$$

208
$$k_3 = hf\left(t_n + \frac{3}{10}h, y_n + \frac{3}{40}k_1 + \frac{9}{40}k_2\right) \tag{17}$$

This peer-reviewed published paper appears as: Akcelyan, S., Lignos, D. G. and Hikino, T. (2018). "Adaptive Numerical Method Algorithms for Nonlinear Viscous and Bilinear Oil Damper Models Subjected to Dynamic Loading". Soil Dynamics and Earthquake Engineering, Vol. 113, pp. 488-502. DOI: 10.1016/j.soildyn.2018.06.021

$$k_4 = hf\left(t_n + \frac{4}{5}h, y_n + \frac{44}{45}k_1 - \frac{56}{15}k_2 + \frac{32}{9}k_3\right) \quad (18)$$

$$k_5 = hf\left(t_n + \frac{8}{9}h, y_n + \frac{19372}{6561}k_1 - \frac{25360}{2187}k_2 + \frac{64448}{6561}k_3 - \frac{212}{729}k_4\right) \quad (19)$$

$$k_6 = hf\left(t_n + h, y_n + \frac{9017}{3168}k_1 - \frac{355}{33}k_2 + \frac{46732}{5247}k_3 + \frac{49}{176}k_4 - \frac{5103}{18656}k_5\right) \quad (20)$$

$$k_7 = hf\left(t_n + h, y_{n+1}\right) \quad (21)$$

Figure 4 shows a flowchart of a single solution step, $i+1$, within a response history analysis of a nonlinear viscous damper. In order to obtain the damper force for the current step, $F_{d,i+1}$, the required input parameters from the overall response history analysis are the integration time step dt_a of the employed integrator for response history analysis (i.e., different than the one employed to obtain the damper force), the velocity of the current and previous steps, $\acute{u}_{i+1}$, $\acute{u}_i$, respectively, and the damper force, $F_{d,i}$ from the previous step, i of the response history analysis. The velocity $\acute{u}$ represents the velocity $\acute{u}_{\mathrm{m}}$ of the Maxwell model. During the initial iteration to compute the damper force, the numerical integration step, h of the DP54 method is set equal to dt_a. If the relative error ε_{rel} is larger than a pre-defined relative tolerance (noted as "RelTol") or if the absolute error is larger than the absolute tolerance (noted as "AbsTol"), the solution algorithm reduces its time step h by half (see Eq. (23)) using a half-step coefficient, s (see Eq. (24)) till Equation (22) is satisfied. In this case, the velocity $\acute{u}_{n+1}$ at the current solution sub-step, which is required from the DP54 iterative method, should be interpolated linearly between $\acute{u}_i$ and $\acute{u}_{i+1}$ at the corresponding sub-step. Therefore, the computation of the acceleration $\ddot{u}_{i+1}$ at the current solution step is needed. Similarly, velocity values within the function evaluations of DP54 iterative method should be linearly interpolated between $\acute{u}_n$ and $\acute{u}_{n+1}$ at the corresponding time increments. As the sum of half-step coefficients s_{tot} becomes equal to unity, we can obtain the damper force at the current solution step, $F_{d,i+1}$. In order to limit the number of iterations N_{it} within the material model, we can introduce a minimum step

This peer-reviewed published paper appears as: Akcelyan, S., Lignos, D. G. and Hikino, T. (2018). "Adaptive Numerical Method Algorithms for Nonlinear Viscous and Bilinear Oil Damper Models Subjected to Dynamic Loading". Soil Dynamics and Earthquake Engineering, Vol. 113, pp. 488-502. DOI: 10.1016/j.soildyn.2018.06.021

size h_{min}. This can simply be done by defining a maximum number of iterations, $N_{it,max}$, for the half step coefficient s as shown in Equation (24).

$$\varepsilon_{rel,n+1} \le \text{RelTol} \quad \text{or} \quad \varepsilon_{n+1} \le \text{AbsTol} \tag{22}$$

$$h = s \cdot dt_a \tag{23}$$

$$s = 2^{-N_{it}}, \qquad N_{it} = \{0,1,2,...,N_{it,\max}\} \tag{24}$$

In order to investigate the effectiveness of the adaptive time step DP54 iterative method on the numerical solution of the force for nonlinear viscous dampers under a sinusoidal displacement excitations, Figure 5 illustrates the force-displacement relation of nonlinear viscous dampers with varying velocity exponents, α (α varies from 0.01 to 2) and normalized damper axial stiffnesses, k_s (i.e., k_s varies from 0.1 to 1000). The sinusoidal displacement that represents the external loading is $u_{m0}\sin(\omega t)$ in which u_{m0} and ω are the peak displacement amplitude and the angular frequency ($\omega = 2\pi f$) of the external loading, respectively. In this case, $u_{mo} = 1$ and $f = 1$ Hz. Referring to Figs. 5 to 8, a 1.0Hz frequency is selected just for the sake of comparisons between computed solutions and experimental results. This frequency is within a typical frequency range of harmonic input excitations that are used for experimental testing of supplemental damping devices (Kasai et al. 2004b). The authors have validated the computed solutions with other meaningful frequency ranges that reflect those typically seen in seismic excitations relative to the employed supplemental damping device characteristics. The overall time step dt_a of the external loading was selected to be $dt_a = 0.01$ sec. The nonlinear viscous damper was designed such that if k_s is neglected then the peak damper force, F_{d0} becomes unity. Thus, F_{d0} can be computed from Equation (25) (i.e., pure viscous dashpot) and therefore, $u_{d0} = u_{m0}$. In this case, the normalized damper stiffness k_s can be obtained from Equation (26). A relative tolerance RelTol = 10^{-6} and an absolute tolerance AbsTol = 10^{-10} are selected herein. The selected threshold for the relative and absolute tolerances is deemed to be small enough for the reliable computation of the numerical solutions of Equations (10) and (11). The selected

This peer-reviewed published paper appears as: Akcelyan, S., Lignos, D. G. and Hikino, T. (2018). "Adaptive Numerical Method Algorithms for Nonlinear Viscous and Bilinear Oil Damper Models Subjected to Dynamic Loading". Soil Dynamics and Earthquake Engineering, Vol. 113, pp. 488-502. DOI: 10.1016/j.soildyn.2018.06.021

values are consistent with prior work on the numerical solution of initial value problems (Griffiths and Higham 2010). More strict convergence criteria could be possibly considered; although the sufficiency of the numerical solution would marginally change, its efficiency would be less given the higher computational cost.

$$F_{d0} = C_d(\omega u_{m0})^{\alpha} \tag{25}$$

$$k_s = K_s \frac{u_{m0}}{F_{d0}} \tag{26}$$

The number of iterations, N_{it} required for the half step coefficient are reported for each case in Figure 5. From this figure, when k_s increases the required number of iterations in order to achieve convergence based on the pre-defined tolerances also increases. From the same figure, the damper exponent α variation has a relatively small influence on the required number of iterations for numerical convergence. The only exception is for $\alpha = 2$, in which a relatively large number of iterations is required to satisfy the pre-defined convergence tolerances (see Figure 5). This is due to the fact that for $\alpha = 2$ the absolute tolerance becomes the critical condition to minimize the error in the damper force prediction, while for all other α values the relative tolerance limits N_{it}. From Figure 5, it is evident that k_s strongly affects the peak damper forces as well as the damper hysteretic shape. These issues are further investigated later on as part of this paper.

In order to illustrate the accuracy of the adaptive integration algorithm for obtaining the hysteretic response of nonlinear viscous dampers compared to traditional iterative numerical methods that have been previously employed, Figure 6 illustrates the force-displacement relations for the same nonlinear viscous dampers that were analyzed in Figure 5 when the classical 4th order RK4 iterative method is employed. Referring to Figure 6, it is evident that when the RK4 iterative method is employed and for $dt_a = 0.01$sec it is not possible to obtain the numerical solution of Equation (10) if $k_s > 10$. Notably, numerical

This peer-reviewed published paper appears as: Akcelyan, S., Lignos, D. G. and Hikino, T. (2018). "Adaptive Numerical Method Algorithms for Nonlinear Viscous and Bilinear Oil Damper Models Subjected to Dynamic Loading". Soil Dynamics and Earthquake Engineering, Vol. 113, pp. 488-502. DOI: 10.1016/j.soildyn.2018.06.021

convergence is achieved for only three α values (i.e., $\alpha = 0.5$, 1.0 and 2.0). In order to obtain a stable numerical solution even in these cases an integration step $dt_a = 0.00005$ sec must be selected.

The adaptive DP54 iterative method can be also implemented for the numerical solution of bilinear oil dampers. In this case, Equation (11) is solved numerically. Note that when $p = 0$ (i.e., constant damper force after relief), $F'_d(t)$ in Equation (11) becomes infinite; therefore the damper force, $F_{d,i+1}$ in this case should be directly equal to F_{dr}. Alternatively, we can compute the damper force $F_{d,i+1}$ through a finite difference approximation of Eq. (11) as follows,

$$F_d(t) = F_{d,i+1} \tag{27}$$

$$\acute{u}_m(t) = \acute{u}_{m,i+1} \tag{28}$$

$$F'_d(t) = \frac{F_{d,i+1} - F_{d,i}}{h} \tag{29}$$

After substituting Equations (27) to (29) into Equation (11), Equation (30) is obtained. First, $F_{d,i+1}$ shall be computed through Equation (30) by assuming that the oil damper is linear (i.e., $|F_{d,i+1}| \le F_{dr}$). If the computed damper force $|F_{d,i+1}| > F_{dr}$, then $F_{d,i+1}$ shall be recomputed using the sign value, $\text{sgn}(F_{d,i+1})$ of the initially computed linear oil damper force prediction.

$$F_{d,i+1} = \begin{cases} \dfrac{F_{d,i} + \acute{u}_{m,i+1} K_s h}{1 + K_s h / C_d}, & |F_{d,i+1}| \le F_{dr} \\ \dfrac{F_{d,i} + \acute{u}_{m,i+1} K_s h + \left[\text{sgn}\left(F_{d,i+1}\right)(1-p) F_{dr} K_s h\right] / \left(p C_d\right)}{1 + K_s h / \left(p C_d\right)}, & |F_{d,i+1}| > F_{dr} \text{ and } p \ne 0 \\ \text{sgn}\left(F_{d,i+1}\right) F_{dr}, & |F_{d,i+1}| > F_{dr} \text{ and } p = 0 \end{cases} \tag{30}$$

Kasai et al. (2004b) recommended that in order to compute the bilinear oil damper force with a high precision, smaller integration steps should be employed. In order to be compatible with the adaptive DP54 iterative method, the error of the numerical solution in this case is defined by subtracting the solution obtained in the current iteration from that of an additional step. For this reason, two numerical solutions

This peer-reviewed published paper appears as: Akcelyan, S., Lignos, D. G. and Hikino, T. (2018). "Adaptive Numerical Method Algorithms for Nonlinear Viscous and Bilinear Oil Damper Models Subjected to Dynamic Loading". Soil Dynamics and Earthquake Engineering, Vol. 113, pp. 488-502. DOI: 10.1016/j.soildyn.2018.06.021

are obtained per iteration, one computed with a time step h_1 and another one with h_2 as shown in Equation (31). Similar to the adaptive DP54 iterative method, for each iteration the integration time step is reduced by half, until the absolute error or the absolute relative error becomes smaller than the predefined tolerances, based on Equation (22).

$$h_1 = s \cdot dt_a, \quad h_2 = s/(s+1) \cdot dt_a \tag{31}$$

In order to compare the adaptive DP54 iterative method with the proposed adaptive numerical integration method (NI) discussed herein for the case of bilinear oil dampers, the force-displacement relations for oil dampers under a sinusoidal external loading with $u_{mo} = 1$ and f = 1 Hz are computed in Figures 7 and 8. The bilinear oil dampers are designed such that their peak force, F_{d0}, becomes unity when the damper axial flexibility is neglected. For bilinear oil dampers, F_{d0} can be computed based on Equation (32). Two cases are analyzed. In the first case, the peak damper velocity ratios are fixed (i.e., $\mu_m = 2$) and p varies from 0 to 1.0 (see Figure 7). In the second case, the p value is fixed (i.e., $p = 0.05$) and μ_m varies from 1 to 20 (see Figure 8). For both cases, the normalized damper axial stiffness, k_s varies from 0.1 to 1000. The relative and absolute tolerances are set equal to RelTol=10^{-6} and AbsTol=10^{-10}, respectively.

$$F_{d0} = \left(p + \frac{1-p}{\mu_m} \right) C_d \omega u_{m0} \tag{32}$$

$$\mu_m = \frac{\omega u_{m0}}{\dot{u}_{dr}} \tag{33}$$

Figure 7 illustrates the computed hysteretic behaviour of bilinear oil dampers with varying p and k_s values based on the adaptive DP54 and finite difference approximation methods. In the same figure we have superimposed the number of iterations, N_{it} required for the half step coefficient based on both iterative methods. From Figure 7 it is concluded that for large k_s values (i.e., $k_s \geq 100$) a small integration time step is required when the adaptive DP54 method is employed; however, this is not the case when the alternative proposed integration scheme is employed. Therefore, for oil dampers that utilize $k_s \geq 100$ the

This peer-reviewed published paper appears as: Akcelyan, S., Lignos, D. G. and Hikino, T. (2018). "Adaptive Numerical Method Algorithms for Nonlinear Viscous and Bilinear Oil Damper Models Subjected to Dynamic Loading". Soil Dynamics and Earthquake Engineering, Vol. 113, pp. 488-502. DOI: 10.1016/j.soildyn.2018.06.021

316 alternative numerical integration method is able to provide the same solution accuracy with the adaptive
317 DP54 iterative method with a smaller number of iterations. For flexible bilinear oil dampers (i.e.,
318 $k_s < 100$) the adaptive DP54 iterative method typically satisfies the pre-defined tolerance criteria with just
319 a single iteration (see Figure 7). Similar conclusions hold true when p is fixed (i.e., $p = 0.05$) and the peak
320 damper velocity ratio, μ_m varies (see Figure 8).
321
322 **5. Sensitivity of Viscous Damper Behaviour to the Damper Axial Stiffness**
323 This section investigates the effect of the axial stiffness, K_s due to viscoelasticity of a viscous damper on
324 its hysteretic behaviour and dynamic stiffnesses based on the proposed adaptive numerical method
325 discussed above. In particular, a sensitivity study is conducted in order to quantify the effect of K_s on the
326 reduction factor of the damper energy dissipation, e_K; the damper peak force, F_{do}; the damper storage
327 stiffness, $K_{m,st}$; and the damper loss stiffness, $K_{m,l}$. A harmonic vibration is assumed for this purpose. A
328 sinusoidal displacement that represents the external loading is applied with $u_{mo} = 1$ and $f = 1$ Hz. The
329 evaluation is conducted in a normalized manner. In particular, similarly with the normalized stiffness k_s
330 (see Equation (26)), the normalized storage and loss stiffnesses $k_{\mathrm{m,st}}$ and $k_{\mathrm{m,l}}$, respectively, can be obtained
331 according to Equation (26). Figure 9 illustrates the graphical definition of these phenomena as well as the
332 dynamic stiffnesses (see Figure 9c). The reduction factor of the damper energy dissipation, e_K is obtained
333 by first computing the area under the corresponding damper hysteresis numerically and then dividing it
334 into the energy produced by the pure viscous model under the same loading conditions. The energy
335 dissipated by nonlinear and bilinear viscous models can be directly computed according to Constantinou
336 and Symans (1993) and Kasai and Nishimura (2004), respectively. The normalized peak damper force f_m
337 is obtained by dividing the peak damper force into the peak force of a pure viscous model, which can be
338 calculated, based on Equations (25) and (32) for nonlinear and bilinear viscous models, respectively.
339 Nonlinear viscous dampers are employed with the utilization of the Maxwell model in order to facilitate

This peer-reviewed published paper appears as: Akcelyan, S., Lignos, D. G. and Hikino, T. (2018). "Adaptive Numerical Method Algorithms for Nonlinear Viscous and Bilinear Oil Damper Models Subjected to Dynamic Loading". Soil Dynamics and Earthquake Engineering, Vol. 113, pp. 488-502. DOI: 10.1016/j.soildyn.2018.06.021

the discussion in the next paragraph. The observations below are general and can be applied to bilinear oil dampers not discussed herein due to brevity.

Figure 10 illustrates the variation of e_K, f_m, $k_{m,st}$ and $k_{m,l}$ (values are normalized as discussed earlier and range between 0 to 1) with respect to the nonlinear viscous damper normalized stiffness k_s for a wide range of α values. From Figure 10, the following observations hold true,

- The change in e_K is relatively large for small α values (see Figure 10a). This is attributed to the fact that the smaller the exponent α, the more stable the damper force becomes with the increase of velocity (see Figure 1a). Therefore, a decrease in external total displacement (i.e. k_s) would mainly affect the dashpot displacement and not that of the spring because the spring force remains relatively constant and the spring displacement is proportional to its force. For instance, when $\alpha = 0$, for $k_s < 1$ the damper hysteretic energy diminishes. For $\alpha = 0$ (i.e., friction dampers) and $\alpha = 1$ (i.e., linear dampers) the reduction factor of the nonlinear viscous damper can be directly computed based on the following equation (Constantinou et al. 1998; Kasai et al. 2003),

$$e_{K,\alpha=0} = \frac{k_s - 1}{k_s}; \quad e_{K,\alpha=1} = \frac{k_s^2}{1 + k_s^2} \tag{34}$$

- From Figure 10b a decrease in k_s has a larger impact on the normalized peak forces (f_m) of a damper with large exponent α (e.g., $\alpha = 1$). Similarly, this is attributed to the fact that the damper force is relatively sensitive to the velocity variation once α becomes large. Therefore, a reduction in the dashpot displacement due to the axial flexibility causes relatively large force reductions when $\alpha = 1$. Note that specifically for friction and linear dampers the peak damper forces can be computed as follows,

$$f_{m,\alpha=0} = k_s; \quad f_{m,\alpha=1} = \frac{k_s}{\sqrt{1 + k_s^2}} \tag{35}$$

This peer-reviewed published paper appears as: Akcelyan, S., Lignos, D. G. and Hikino, T. (2018). "Adaptive Numerical Method Algorithms for Nonlinear Viscous and Bilinear Oil Damper Models Subjected to Dynamic Loading". Soil Dynamics and Earthquake Engineering, Vol. 113, pp. 488-502. DOI: 10.1016/j.soildyn.2018.06.021

- The normalized storage stiffness $k_{m,st}$ is large for small α values; $k_{m,st}$ becomes maximum when $k_s = 1$ (see Figure 10c). This implies that although the inclination angle of the damper hysteresis is small for $k_s < 1$ (see Figure 5), the $k_{m,st}$ is relatively small due to fact that the normalized peak forces, f_m significantly decrease for $k_s < 1$ as shown in Figure 10b. For $k_s > 1$ the $k_{m,st}$ reduces due to the changing shape of the damper hysteresis. For large k_s values the damper hysteresis becomes similar to that of a pure viscous model, which has no storage stiffness. For friction and linear dampers the normalized storage stiffness can be computed as follows,

$$k_{m,st,\alpha=0} = k_s; \quad k_{m,st,\alpha=1} = \frac{k_s}{1+k_s^2} \tag{36}$$

- From Figure 10d the normalized loss stiffness, $k_{m,l}$ increases with the increase of k_s. Under the same loading conditions, a pure viscous model would have a normalized loss stiffness $k_{m,l} = 1$, because the maximum force occurs at zero displacement; thus the larger the k_s, the larger the $k_{m,l}$ becomes. Note that Equation (37) can be employed to compute the normalized loss stiffness for friction and linear dampers,

$$k_{m,l,\alpha=0} = k_s - 1; \quad k_{m,l,\alpha=1} = \frac{k_s^2}{1+k_s^2} \tag{37}$$

Figure 10 can facilitate the design and modeling of the damper stiffness. For instance, Figure 10a suggests that if the damper has a normalized stiffness $k_s > 100$, it is practically a pure viscous model, while for $k_s = 10$ the energy dissipation is about 90% of that of a viscous model for a low velocity exponent. If $k_s < 10$, the loss in energy dissipation increases dramatically. When $\alpha \approx 0$ the damper hysteretic energy diminishes for $k_s < 1$. These graphs can be utilized to accelerate the preliminary evaluation procedures within a building model. If the damper stiffness properties are unknown, Figure 10 can be used to easily assign a damper stiffness, that is computationally efficient (not too stiff) and at the same time reasonably conservative (i.e. not too flexible) for the evaluation of a building's engineering demand parameters. This

This peer-reviewed published paper appears as: Akcelyan, S., Lignos, D. G. and Hikino, T. (2018). "Adaptive Numerical Method Algorithms for Nonlinear Viscous and Bilinear Oil Damper Models Subjected to Dynamic Loading". Soil Dynamics and Earthquake Engineering, Vol. 113, pp. 488-502. DOI: 10.1016/j.soildyn.2018.06.021

should aid eliminating analysis iterations with unnecessarily too stiff or too flexible damper models. Note that, an estimation of the building's fundamental frequency and peak damper displacement (u_{m0}) is sufficient to compute the required damper stiffness that satisfies the selected k_s (see Eq. 26). Similar expressions can be derived for bilinear oil dampers.

6. Experimental Validation

This section discusses the validation of the proposed adaptive integration techniques for the numerical models of nonlinear viscous and bilinear oil dampers. The validation is conducted with damper component experiments conducted in prior studies. System-level experimental data from a full-scale shake table test of a 5-story steel frame building with nonlinear viscous and bilinear oil dampers are also utilized.

6.1. *Component Level Validation*

Component level experiments for both nonlinear viscous and oil dampers are adopted from earlier experimental studies (Kasai et al. 2004b; Ooki et al. 2009; Hikino 2012). The nonlinear viscous damper that was tested had a viscous coefficient, C_d = 196 KN/(mm/s)$^{0.38}$, axial stiffness, K_d = 438 KN/mm and a damper exponent, α = 0.38. The nonlinear viscous damper was subjected to sinusoidal loading with increasing displacement amplitudes and loading frequencies of 0.5Hz and 2Hz, respectively. Figure 11 illustrates the measured hysteretic response of the nonlinear viscous damper in terms of its force-displacement relation for the two loading frequencies of interest. In the same figure, we have superimposed the computed hysteretic response of the nonlinear viscous damper based on a Maxwell model. For the numerical solution of the constitutive equation of the Maxwell model with the proposed adaptive numerical technique an integration step of 0.01sec is adopted. The adaptive DP54 method required 3 iterations (i.e. h = 0.00125 sec) to satisfy the pre-defined convergence criteria (i.e., 10^{-6} and 10^{-}

This peer-reviewed published paper appears as: Akcelyan, S., Lignos, D. G. and Hikino, T. (2018). "Adaptive Numerical Method Algorithms for Nonlinear Viscous and Bilinear Oil Damper Models Subjected to Dynamic Loading". Soil Dynamics and Earthquake Engineering, Vol. 113, pp. 488-502. DOI: 10.1016/j.soildyn.2018.06.021

^{10} for the relative and absolute tolerances, respectively). From Figure 11, the average absolute relative error of the predicted positive and negative peak damper forces per loading cycle versus the measured ones is 9% and 6% for 0.5 and 2.0Hz, respectively. This suggests that the proposed numerical model for nonlinear viscous dampers represents well the experimental data regardless of the employed loading frequency.

Similarly, for bilinear oil dampers the experimental data from Kasai et al. (2004b) is utilized. In this case, the bilinear oil damper that was tested dynamically at full-scale had an initial damper coefficient, C_d = 24.5 KN/(mm/s), an axial stiffness, K_d = 392.3 KN/mm, a relief velocity, $\acute{u}_{dr}$ = 32 mm/s, and a post-relief coefficient ratio, p = 0.068 (Takahashi and Sekiguchi 2001). The bilinear oil damper was subjected to sinusoidal loading with increasing displacement amplitude of 1, 5 and 15 mm and loading frequencies of 0.25 Hz and 1 Hz. Figure 12 illustrates the measured hysteretic response of the bilinear oil damper for the two loading frequencies of interest. From Figure 3.12a, at 0.25 Hz the relief valve of the oil damper was not activated; therefore, the damper response was linear. However, at 1Hz and during the last loading cycle (i.e., displacement amplitude of 15 mm) the damper relief velocity was exceeded. Thus, a bilinear force-velocity relation was measured as shown in Figure 12b. In the same figure we have superimposed the computed hysteretic response of the same damper. The integration step of the proposed adaptive numerical technique that was employed was 0.01 sec. The adaptive DP54 method required 5 iterations (i.e. h = 0.0003125 sec) to satisfy the pre-defined convergence criteria (i.e., 10^{-6} and 10^{-10} for the relative and absolute tolerances, respectively). Referring to Figure 12, the computed hysteretic response of the oil damper is nearly identical with the one obtained from the experimental data regardless of the loading frequency. This is also indicated from the average absolute error of positive and negative peak damper forces per loading cycle that was 5% and 3% for 0.25 Hz and 1 Hz, respectively.

This peer-reviewed published paper appears as: Akcelyan, S., Lignos, D. G. and Hikino, T. (2018). "Adaptive Numerical Method Algorithms for Nonlinear Viscous and Bilinear Oil Damper Models Subjected to Dynamic Loading". Soil Dynamics and Earthquake Engineering, Vol. 113, pp. 488-502. DOI: 10.1016/j.soildyn.2018.06.021

6.2. *Validation with System-Level Experimental Data*

This section discusses the implementation of the proposed adaptive integration techniques for simulating the hysteretic response of nonlinear viscous and bilinear oil dampers based on the utilization of full-scale shake table experiments of a 5-story steel frame building that was tested at the world's largest shake table at E-Defense in Japan (Ohtani et al. 2004; Kasai et al. 2008; Kasai et al. 2010; Hikino 2012; Kasai and Matsuda 2014). The test structure was equipped various types of dampers including nonlinear viscous and bilinear oil dampers (Ooki et al. 2009; Kasai et al. 2010; Hikino 2012). The employed numerical models including the adaptive integration techniques (noted as "ViscousDamper" and "BilinearOilDamper") discussed in this paper have been implemented in an open-source finite element simulation platform for nonlinear response history analysis of 2- and 3-Dimensional frame buildings under earthquake excitations [so called: Open System for Earthquake Engineering Simulation (*OpenSees*), (McKenna 1997)]. These models including their documentation are publically available (BilinearOilDamper 2015; ViscousDamper 2015).

Figure 13a shows the test structure after the installation on the E-Defense shake table. The test structure plan view was 10x12 m as (see Figure 13b). Its total height was 15.85 m and its overall weight was 4730 KN. Detailed information regarding the test structure is reported extensively elsewhere (Ooki et al. 2009; Kasai et al. 2010; Kasai and Matsuda 2014). Due to brevity, the reader is referred to the aforementioned studies.

Twelve dampers were installed in the test structure in total (four in the Y-loading direction; eight in the X-loading direction) as shown in Figures 13c and 13d. Table 1 provides the various properties of the nonlinear viscous and bilinear oil dampers based on damper component tests prior to the shake table experiments. In summary, Table 1 includes the damping coefficients, C_d, the stiffness properties (i.e., damper portion, K_d and total stiffness K_s) of the corresponding dampers installed in the test structure. The velocity exponent, α, of the nonlinear viscous dampers was found to be, $\alpha = 0.38$. The relief velocity, $\acute{u}_{dr}$

This peer-reviewed published paper appears as: Akcelyan, S., Lignos, D. G. and Hikino, T. (2018). "Adaptive Numerical Method Algorithms for Nonlinear Viscous and Bilinear Oil Damper Models Subjected to Dynamic Loading". Soil Dynamics and Earthquake Engineering, Vol. 113, pp. 488-502. DOI: 10.1016/j.soildyn.2018.06.021

and post relief damping coefficient ratio, p of the bilinear oil dampers were found to be, $\acute{u}_{dr}$ = 64 mm/sec and p = 0.068, respectively (Kasai et al. (2008); Ooki et al. (2009); Hikino 2012).

The test structure was subjected to the three components of the JR Takatori record from the 1995 Kobe earthquake. These components were scaled incrementally at 50%, and 100% of the unscaled intensity of the same ground motion. Further details regarding the testing program can be found in Kasai and Matsuda (2014).

A 3-Dimensional (3D) model of the test structure was developed in the *OpenSees* simulation platform. The steel beams and columns were modeled with a single force-based distributed plasticity beam-column element with five integration points along their length. In order to trace flexural yielding within the cross sections a combined isotropic/kinematic material model (Menegotto and Pinto 1973) was assigned to the fiber-based cross sections that were assigned to the force-based nonlinear beam-column elements. The fiber discretization of each cross section consisted of 5x3 fiber elements along the width and thickness of flanges and webs, respectively. The measured material properties reported by (Kasai and Matsuda 2014) were explicitly assigned to the various steel beam and columns of the test structure. The reinforced concrete slab on top of the steel beams was modeled with a concrete material (Yassin 1994), which accounts for the effect of linear tension softening of the concrete. The effective width of the concrete slab was calculated based on Section I3.1a of ANSI/AISC 360-10 (AISC 2010). Rigid diaphragms were assigned at each floor level. The P-Delta transformation was assigned to the steel members of the test structure to simulate the second order effects. The viscous damping forces of the test structure were simulated with the Rayleigh model. In particular, 2% damping ratio was assigned to the first and third modes of the 3-D model. Two seismic intensities (50% and 100%) were considered for the evaluation presented herein. Nonlinear response history analysis with direct integration of the equations of motion was conducted. The Newmark's average acceleration method (Newmark 1959) was used for this purpose.

This peer-reviewed published paper appears as: Akcelyan, S., Lignos, D. G. and Hikino, T. (2018). "Adaptive Numerical Method Algorithms for Nonlinear Viscous and Bilinear Oil Damper Models Subjected to Dynamic Loading". Soil Dynamics and Earthquake Engineering, Vol. 113, pp. 488-502. DOI: 10.1016/j.soildyn.2018.06.021

The integration time step was taken equal to dt=0.01 sec. A detailed summary of the developed numerical model of the test structure can be found in Lignos (2012) and (Akcelyan et al. 2016).

Figure 14 shows a comparison of the measured (noted as Test-50 and Test-100) and computed absolute peak values of story drift ratios, story shear forces and floor absolute accelerations along the height of the test structure with nonlinear viscous dampers under 50% and 100% of the unscaled Takatori record in both loading directions (i.e., directions X and Y). In order to illustrate the efficiency of the adaptive integration techniques for the numerical solution of viscous dampers including their axial flexibility, two types of nonlinear response history analyses are carried out. In the first one (noted as NRHA1) the axial flexibility of the dampers is neglected. In the second one (noted as NRHA2) the axial flexibility of the damper is considered. Note that the average absolute errors of global peak engineering demand parameters (EDPs) shown in Figure 14 increase from 7% to 27% when the axial flexibility of the damper is disregarded. In the Y-loading direction, the average absolute errors along the height of the test structure are much larger than those in the X-loading direction. In particular, the predicted peak EDPs are underestimated by more than 45% in average. Referring to Figure 15, nearly identical findings hold true for the test structure with oil dampers. These simple comparisons indicate the importance of rigorous mathematical models, such as the nonlinear Maxwell model, to accurately represent the hysteretic response of viscous dampers including their axial flexibility. In this case, the advantage of the proposed adaptive numerical method techniques to overcome typical convergence problems during nonlinear response history analyses of large-scale finite element models with fairly large integration steps is also pronounced.

Figure 16 illustrates the measured hysteretic response of the damper portion (K_d and C_d) of the nonlinear viscous and bilinear oil dampers installed in the first story of the test structure in X- and Y- loading directions, respectively, for the 100% seismic intensity of the JR Takatori record. In the same figure we have superimposed the simulated hysteretic response of the same components based on NRHA of the 3D

This peer-reviewed published paper appears as: Akcelyan, S., Lignos, D. G. and Hikino, T. (2018). "Adaptive Numerical Method Algorithms for Nonlinear Viscous and Bilinear Oil Damper Models Subjected to Dynamic Loading". Soil Dynamics and Earthquake Engineering, Vol. 113, pp. 488-502. DOI: 10.1016/j.soildyn.2018.06.021

model representation of the test structure with nonlinear viscous dampers and bilinear oil dampers based on the proposed adaptive integration techniques discussed in this paper. From Figure 16 it is evident that in both cases the proposed numerical models are rational and are able to capture fairly well both the peak damper forces as well as the damper displacement amplitudes.

The efficiency of the presented algorithms in computing the numerical solutions of the damper devices presented herein has been also evaluated in cases that steel frame buildings retrofitted with nonlinear viscous dampers exhibit inelastic behavior during severe ground motion shaking (Akcelyan 2017, Akcelyan and Lignos 2018, Wang and Mahin, 2017). It was found in all cases that the proposed numerical schemes have excellent convergence characteristics.

7. Summary and Conclusions

This paper discusses the implementation of advanced adaptive numerical integration algorithms for the numerical solution of the constitutive equations that describe the force-displacement relation of viscous dampers under random vibrations. The integration schemes are implemented in an open source finite element analysis program in order to calculate fourth- and fifth-order accurate numerical solutions of a damper force under dynamic loading when the axial flexibility of the respective viscous damper is considered in the mathematical model representation of the damper. Through a sensitivity study, the efficiency of the adaptive integration algorithm over traditional integration schemes for the numerical solution of initial value problems is demonstrated. In particular, it is shown that even in cases that involve nonlinear viscous dampers with large axial stiffness and small velocity exponents a high-accuracy numerical solution of the force-displacement relations of the respective damper is achieved with relatively large integration steps and only few sub-step iterations. In the case of bilinear oil dampers with large axial stiffness an alternative adaptive numerical integration algorithm is also proposed. This integration scheme is able to provide same accuracy solutions with the adaptive Dormand-Prince iterative method but with

This peer-reviewed published paper appears as: Akcelyan, S., Lignos, D. G. and Hikino, T. (2018). "Adaptive Numerical Method Algorithms for Nonlinear Viscous and Bilinear Oil Damper Models Subjected to Dynamic Loading". Soil Dynamics and Earthquake Engineering, Vol. 113, pp. 488-502. DOI: 10.1016/j.soildyn.2018.06.021

much smaller number of sub-step iterations. The employed integration schemes allow for the investigation of the sensitivity of the viscous damper behaviour to its axial stiffness. The adaptive integration schemes for the numerical solution of the nonlinear Maxwell model are validated through a series of comparisons with damper component tests as well as system-level experimental data from full-scale shake table tests of a 5-story steel frame building with nonlinear viscous and bilinear oil dampers. The validation studies underscore the efficiency of the proposed integration schemes in predicting the global and local engineering demand parameters of frame buildings equipped with supplemental damping devices at a relatively low computational cost.

Acknowledgements

The authors express their sincere thanks to the research team who conducted the full-scale shake table tests of the 5-story steel frame building with various types of dampers (Leader: Professor Kazuhiko Kasai, Tokyo Institute of Technology) and to the National Research Institute for Earth Science and Disaster Prevention for providing the experimental data for the needs of this paper. The authors also acknowledge the financial support from Fonds de recherche du Québec Nature et technologies (Grant No. 2013 – NC-166845). The findings in this paper are those of the authors and do not necessary reflect the view of the sponsors.

References

AISC (2010). "Specification for structural steel buildings." *ANSI/AISC 360-10*, American Institute of Steel Construction, Chicago, IL.

Akcelyan, S., Lignos, D. G., Hikino, T., and Nakashima, M. (2016). "Evaluation of simplified and state-of-the-art analysis procedures for steel frame buildings equipped with supplemental damping devices based on E-Defense full-scale shake table tests." *Journal of Structural Engineering*, 142(6), 04016024.

Akcelyan, S., and Lignos, D.G. (2018). "Seismic retrofit of steel tall buildings with bilinear oil dampers." *Proc., 16th European Conference on Earthquake Engineering*, Thessaloniki, Greece, 18-21 June 2018.

BilinearOilDamper (2015). "BilinearOilDamper material." *OpenSeesWiki online manual*, <http://opensees.berkeley.edu/wiki/index.php/BilinearOilDamper_Material>. (Aug. 6, 2015).

Black, C., and Makris, N. (2007). "Viscous heating of fluiddampers under small and large amplitude motions: experimental studies and parametric modeling." *Journal of Engineering Mechanics*, 133(5), 566-577.

Buchanan, A., Bull, D., Dhakal, R., MacRae, G., Palermo, A., and Pampanin, S. (2011). "Base isolation and damage-resistant technologies for improved seismic performance of buildings: A report written for the Royal Commission of Inquiry into building failure caused by the Canterbury earthquakes." *Research Report 2011-02*, Department of Civil and Natural Resources Engineering, University of Canterbury, Christchurch.

Butcher, J. C. (1996). "A history of Runge-Kutta methods." *Applied Numerical Mathematics*, 20(3), 247-260.

Chang, K. C., Soong, T. T., Oh, S.-T., and Lai, M. L. (1995). "Seismic behavior of steel frame with added viscoelastic dampers." *Journal of Structural Engineering*, 121(10), 1418-1426.

Chen, Y.-T., and Chai, Y. H. (2011). "Effects of brace stiffness on performance of structures with supplemental Maxwell model-based brace–damper systems." *Earthquake Engineering & Structural Dynamics*, 40(1), 75-92.

Christopoulos, C., and Filiatrault, A. (2006). *Principles of supplemental damping and seismic isolation*, IUSS Press, Milan, Italy.

Constantinou, M., Tsopelas, P., Hammel, W., and Sigaher, A. (2001). "Toggle-brace-damper seismic energy dissipation systems." *Journal of Structural Engineering*, 127(2), 105-112.

Constantinou, M. C., Soong, T. T., and Dargush, G. F. (1998). "Passive energy dissipation systems for structural design and retrofit." *MCEER-Monograh No: 1*, Multidisciplinary Center for Earthquake Engineering Research, University of Buffalo., USA.

Constantinou, M. C., and Symans, M. D. (1993). "Experimental study of seismic response of buildings with supplemental fluid dampers." *The Structural Design of Tall Buildings*, 2(2), 93-132.

Diotallevi, P. P., Landi, L., and Dellavalle, A. (2012). "A methodology for the direct assessment of the damping ratio of structures equipped with nonlinear viscous dampers." *Journal of Earthquake Engineering*, 16(3), 350-373.

Dong, B., Sause, R., and Ricles, J. M. (2015). "Accurate real-time hybrid earthquake simulations on large-scale MDOF steel structure with nonlinear viscous dampers." *Earthquake Engineering & Structural Dynamics*, 44(12), 2035-2055.

Dong, B., Sause, R., and Ricles, J.M. (2018). "Seismic erformance of steel MRF structures with nonlinear viscous dampers from real-time hybrid simulations." *Proc., 9th International Conference on the Behaviour of Steel Structures in Seismic Areas*, Christchurch, New Zealand, February 14-17, 2018.

Dormand, J. R., and Prince, P. J. (1980). "A family of embedded Runge-Kutta formulae." *Journal of Computational and Applied Mathematics*, 6(1), 19-26.

592 Griffiths, D., Higham, D.J. (2010). “Numerical methods for ordinary differential equations – Initial value
593 problems”, S*pringer Series ISBN 978-0-85729-148-6.*
594 Hairer, E., Norsett, E., Wanner, G. (1993). “Solving ordinary differential equations I – Nonstiff
595 problems”, *Springler Series in Computational Mathematics*.
596 Hikino, T. (2012). "Full-scale shaking table test and analysis of the dynamic characteristics verification
597 that govern the seismic behavior of steel buildings with supplemental damping." Ph.D.
598 Dissertation, Kyoto University, Japan (in Japanese).
599 Hwang, J., Huang, Y., Yi, S., and Ho, S. (2008). "Design formulations for supplemental viscous dampers
600 to building structures." *Journal of Structural Engineering*, 134(1), 22-31.
601 Ichihasi, S., Okuzono, T., Takahashi, O., Usami, M., Ninomiya, M., Tsuyuki, Y., and Ishida, Y. (2000).
602 "Vibration test of a frame which has an oil-damper brace." *Proc., The 12th World Conference on*
603 *Earthquake Engineering (WCEE)*, Auckland, New Zealand.
604 Kasai, K., Ito, H., Ooki, Y., Hikino, T., Kajiwara, K., Motoyui, S., Ozaki, H., and Ishii, M. (2010). "Full-
605 scale shake table tests of 5-story steel building with various dampers." *Proc., 7th International*
606 *Conference on Urban Earthquake Engineering (7CUEE) & 5th International Conference on*
607 *Earthquake Engineering (5ICEE)*, Tokyo Institute of Technology, Tokyo, Japan.
608 Kasai, K., and Matsuda, K. (2014). "Full-scale dynamic testing of response-controlled buildings and their
609 components: concepts, methods, and findings." *Earthq. Engin. Engin. Vib.*, 13(1), 167-181
610 English.
611 Kasai, K., Mita, A., Kitamura, H., Matsuda, K., Morgan, T. A., and Taylor, A. W. (2013). "Performance
612 of seismic protection technologies during the 2011 Tohoku-Oki Earthquake." *Earthquake*
613 *Spectra*, 29(S1), S265-S293.
614 Kasai, K., and Nishimura, T. (2004). "Equivalent linearization of passive control system with oil damper
615 bilinearly dependent on velocity." *Journal of Structural and Construction Engineering, AIJ,*
616 (583), 47-54 (in Japanese).
617 Kasai, K., Ogura, T., and Suzuki, A. (2007). "Passive control desing method based on tuning equivalent
618 stiffness of nonlinear viscous dampers." *Journal of Structural and Construction Engineering, AIJ,*
619 , 76(618), 97-104 (in Japanese).
620 Kasai, K., Oohara, K., and Sekiguchi, Y. (2004). "JSSI manual for building passive control technology
621 part-10 time-history analysis model for viscous dampers." *Proc., The 13th World Conference on*
622 *Earthquake Engineering*, Vancouver, B.C., Canada.
623 Kasai, K., Ooki, Y., Ishii, M., Ozaki, H., Ito, H., Motoyui, S., Hikino, T., and Sato, E. (2008). "Value-
624 added 5-story steel frame and its components: Part 1 - Full-scale damper tests and analyses."
625 *Proc., The 14th World Conference on Earthquake Engineering*, Beijing, China.
626 Kasai, K., Suzuki, A., and Oohara, K. (2003). "Equivalent linearization of a passive control system
627 having viscous dampers dependent on fractional power of velocity." *Journal of Structural and*
628 *Construction Engineering, AIJ,*(574), 77-84 (in Japanese).
629 Kasai, K., Takahashi, O., and Sekiguchi, Y. (2004). "JSSI manual for building passive control technology
630 part-10 time-history analysis model for nonlinear oil dampers." *Proc., The 13th World Conference*
631 *on Earthquake Engineering*, Vancouver, B.C., Canada.
632 Kutta, W. (1901). "Beitrag zur näherungsweisen Integration totaler Differentialgleichungen." *Zeitschrift*
633 *für Mathematik und Physik*, 46, 435-453.
634 Lavan, O., and Avishur, M. (2013). "Seismic behavior of viscously damped yielding frames under
635 structural and damping uncertainties." *Bull Earthquake Eng*, 11(6), 2309-2332 English.
636 Lavan, O., Cimellaro, G., and Reinhorn, A. (2008). "Noniterative optimization procedure for seismic
637 weakening and damping of inelastic structures." *Journal of Structural Engineering*, 134(10),
638 1638-1648.
639 Liang, Z., Lee, G. C., and Dargush, G. F. (2011). *Structural damping: Applications in seismic response*
640 *modification*, CRC Press, USA.

Lignos, D. G. (2012). "Modeling and experimental validation of a full scale 5-story steel building equipped with tripple friction pendulum bearings: E-defense blind analysis competition." *Proc., 9th International Conference on Urban Earthquake Engineering (9CUEE) & 4th Asia Conference on Earthquake Engineering, Center for Urban Earthquake Engineering (CUEE)*, Tokyo Institute of Technology, Tokyo.

Lin, W.-H., and Chopra, A. K. (2002). "Earthquake response of elastic SDF systems with non-linear fluid viscous dampers." *Earthquake Engineering & Structural Dynamics*, 31(9), 1623-1642.

Londoño, J. M., Neild, S. A., and Wagg, D. J. (2013). "A noniterative design procedure for supplemental brace–damper systems in single-degree-of-freedom systems." *Earthquake Engineering & Structural Dynamics*, 42(15), 2361-2367.

Makris, N., and Constantinou, M. (1991). "Fractional‐derivative maxwell model for viscous dampers." *Journal of Structural Engineering*, 117(9), 2708-2724.

Maxwell, J. C. (1867). "On the dynamical theory of gases." *Philosophical Transactions of the Royal Society of London*, 157, 49-88.

McKenna, F. T. (1997). "Object-oriented finite element programming: frameworks for analysis, algorithms and parallel computing." Ph.D. Dissertation, University of California, Berkeley.

Menegotto, M., and Pinto, P. E. (1973). "Method of analysis for cyclically loaded reinforced concrete plane frames including changes in geometry and non-elastic behaviour of elements under combined normal force and bending." *Proc., IABSE, Symp. on Resistance and Ultimate Deformability of Structures Acted on by Well Defined Repeated Loads, IABSE-AIPC-IVBH*, ETH Zurich, Zurich, Switzerland, 15-22.

Miranda, E., Mosqueda, G., Retamales, R., and Pekcan, G. (2012). "Performance of nonstructural components during the 27 February 2010 Chile Earthquake." *Earthquake Spectra*, 28(S1), S453-S471.

Newmark, N. M. (1959). "A method of computation for structural dynamics." *Journal of the Engineering Mechanics Division, ASCE*, 85(3), 67-94.

Ohtani, K., Ogawa, N., Katayama, T., and Shibata, H. (2004). "Construction of E-Defense (3-D full-scale earthquake testing facility)." *Proc., 13th World Conference on Earthquake Engineering*, Vancouver, B.C., Canada.

Oohara, K., and Kasai, K. (2002). "Time history analysis models for nonlinear viscous dampers." *Proc., Structural Engineers World Congress (SEWC)*, Yokohama, JAPAN.

Ooki, Y., Kasai, K., Motoyui, S., Kaneko, K., Kajiwara, K., and Hikino, T. (2009). "Full-scale tests of passively-controlled 5-story steel building using E-Defense shake table part 3: full-scale tests for dampers and beam-column subassemblies." *Proc., STESSA 2009*, Philadelphia, 93-99.

Pall, A. S., and Marsh, C. (1982). "Response of friction damped braced frames." *Journal of the Structural Division, ASCE*, 108(6), 1313-1323.

Pekcan, G., Mander, J. B., and Chen, S. S. (1999). "Fundamental considerations for the design of non‐linear viscous dampers." *Earthquake Engineering & Structural Dynamics*, 28(11), 1405-1425.

Pollini, N., Lavan, O., and Amir, O. (2017). "Minimum-cost optimization of nonlinear fluid viscous dampers and their supporting members for seismic retrofitting." *Earthquake Engineering & Structural Dynamics*, n/a-n/a.

Ramirez, O. M., Constantinou, M. C., Kircher, C. A., Whittaker, A. S., Johnson, M. W., Gomez, J. D., and Chrysostomou, C. Z. (2001). "Development and evaluation of simplified procedures for analysis and design of buildings with passive energy dissipation systems." *MCEER-00-0010 2001*, Multidisciplinary Center for Earthquake Engineering Research, University of Buffalo, USA.

Reinhorn, A. M., Li, C., and Constantinou, M. C. (1995). "Experimental & analytical investigation of seismic retrofit of structures with supplemental damping, Part 1: Fluid viscous damping devices."

NCEER-95-0001, National Center for Earthquake Engineering Research, University of Buffalo, USA.

Singh, M., Verma, N., and Moreschi, L. (2003). "Seismic analysis and design with maxwell dampers." *Journal of Engineering Mechanics*, 129(3), 273-282.

Sivaselvan, M. V., Lavan, O., Dargush, G.F., Kurino, H., Hyodo, Y., Fukuda, R., Sato, K., Apostolakis, G., and Reinhorn, A.M. (2009). "Numerical collapse simulation of large-scale structural systems using an optimization-based algorithm."*Earthquake Engineering and Structural Dynamics*, 38 (5), 655-677.

Soong, T., and Dargush, G. (1997). *Passive energy dissipation systems in structural engineering*, John Wiley & Sons, Chichester, United Kingdom.

Symans, M., Charney, F., Whittaker, A., Constantinou, M., Kircher, C., Johnson, M., and McNamara, R. (2008). "Energy dissipation systems for seismic applications: current practice and recent developments." *Journal of Structural Engineering*, 134(1), 3-21.

Symans, M. D., and Constantinou, M. C. (1998). "Passive fluid viscous damping systems for seismic energy dissipation." *ISET Journal of Earthquake Technology*, 35(4), 185-206.

Takahashi, O., and Sekiguchi, Y. (2001). "Constitutive rule of oil damper with maxwell model and source code for analysis program." *Proc., Passively Controlled Structure Symposium 2001*, Yokohama, Japan.

Terenzi, G. (1999). "Dynamics of SDOF systems with nonlinear viscous damping." *Journal of Engineering Mechanics, ASCE*, 125 (8), 956-963.

Tsuyuki, Y., Gofuku, Y., Iiyama, F., and Kotake, Y. (2004). "JSSI manual for building passive control technology part-3 performance and quality control of oil damper." *Proc., The 13th World Conference on Earthquake Engineering*, Vancouver, B.C., Canada.

ViscousDamper (2015). "ViscousDamper material." *OpenSeesWiki online manual*, <http://opensees.berkeley.edu/wiki/index.php/ViscousDamper_Material>. (Sep. 30, 2016).

Wang, S., and Mahin, S.A. (2017). "Seismic retrofit of a high-rise steel moment-resisting frame using fluid viscous dampers." The Structural Design of Tall and Special Buildings, 26 (10), 1-11.

Yassin, M. H. M. (1994). "Nonlinear analysis of prestressed concrete structures under monotonic and cycling loads." Ph.D. Dissertation, University of California, Berkeley.

Yu, Y., Tsai, K., Li, C., Weng, Y., and Tsai, C. (2013). "Earthquake response analyses of a full-scale five-story steel frame equipped with two types of dampers." *Earthquake Engineering & Structural Dynamics*, 42(9), 1301-1320.

722 **Table 1:** Properties of nonlinear viscous dampers and oil dampers (Hikino, 2012).

		Nonlinear Viscous Damper (α = 0.38)			Oil Damper ($\dot{u}_{dr}$ = 64 mm/s, p = 0.068)		
Frame	Story	C_d [KN/(mm/s)$^{0.38}$]	K_d [KN/mm]	K_s [KN/mm]	C_d [KN/(mm/s)]	K_d [KN/mm]	K_s [KN/mm]
X direction (2 bays)	4	49	119[(a)]	60	3.13	88	57
	3	49	119[(a)]	60	6.25	137	85
	2	98	193	104	6.25	137	85
	1	98	193	101	12.5	274	146
Y direction (1 bay)	4	98	193	104	6.25	137	85
	3	98	193	104	12.5	274	154
	2	196	438	179	12.5	274	154
	1	196	438	171	18.75	441	242

723 (a) Estimated stiffness values (K_d) for damper portion due to lack of data of dampers at third and fourth story (Yu et

724 al. 2013).

725

726

727

728

729

730 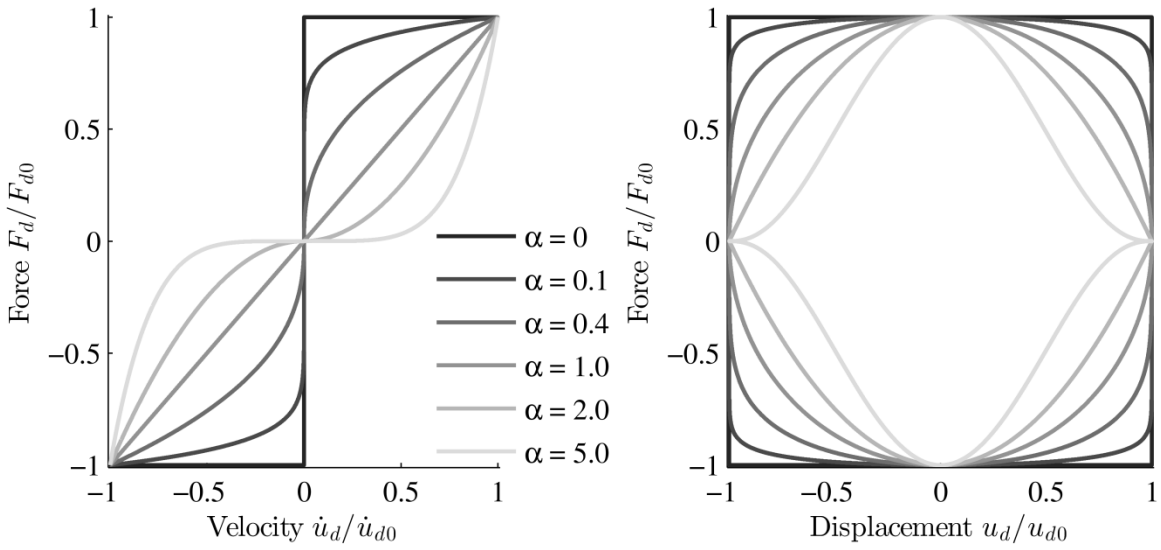

(a) Force - velocity relation (b) Force - displacement relation

731

732 **Figure 1:** Hysteretic behaviour of nonlinear viscous dampers with various velocity exponents under

733 sinusoidal motion

734

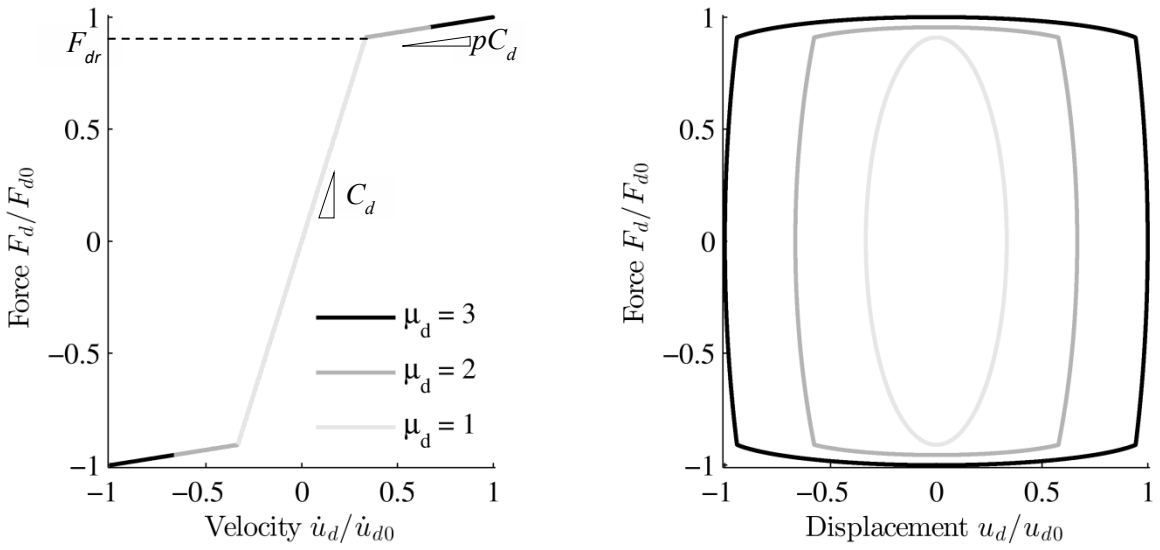

735

(a) Force - velocity relation (b) Force - displacement relation

736

737 **Figure 2:** Hysteretic behaviour of bilinear oil dampers under sinusoidal motion with increasing loading

738 amplitudes

739

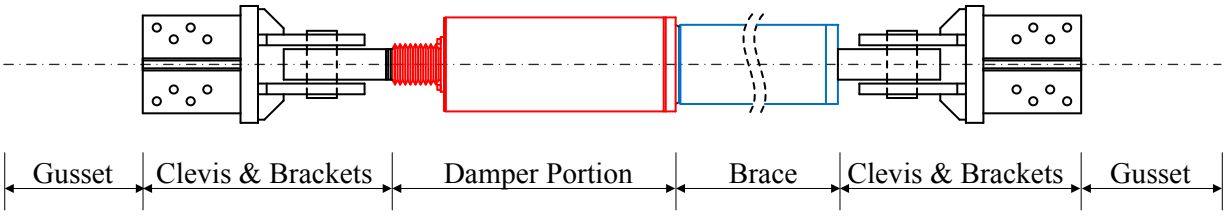

(a) Nonlinear viscous damper

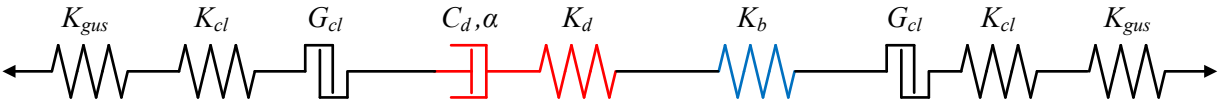

(b) Mechanical model for nonlinear viscous damper

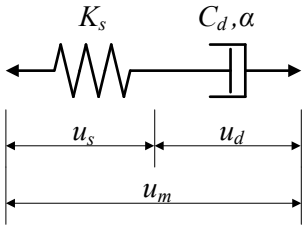

(c) Maxwell model

740
741 **Figure 3:** Schematic representation of nonlinear viscous damper including its mathematical model

742

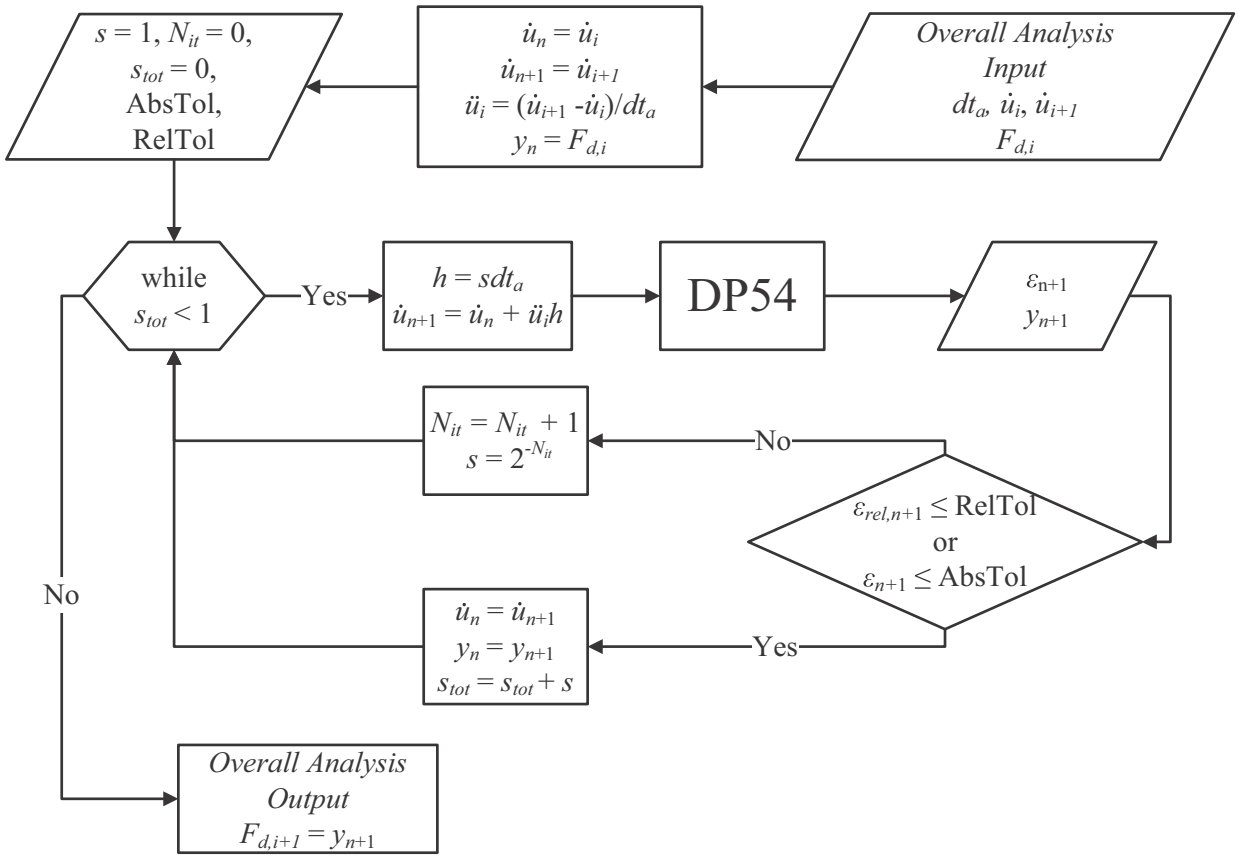

743

744 **Figure 4:** Flow chart of the numerical solution based on the adaptive DP54 explicit iterative method for

745 nonlinear viscous dampers

746

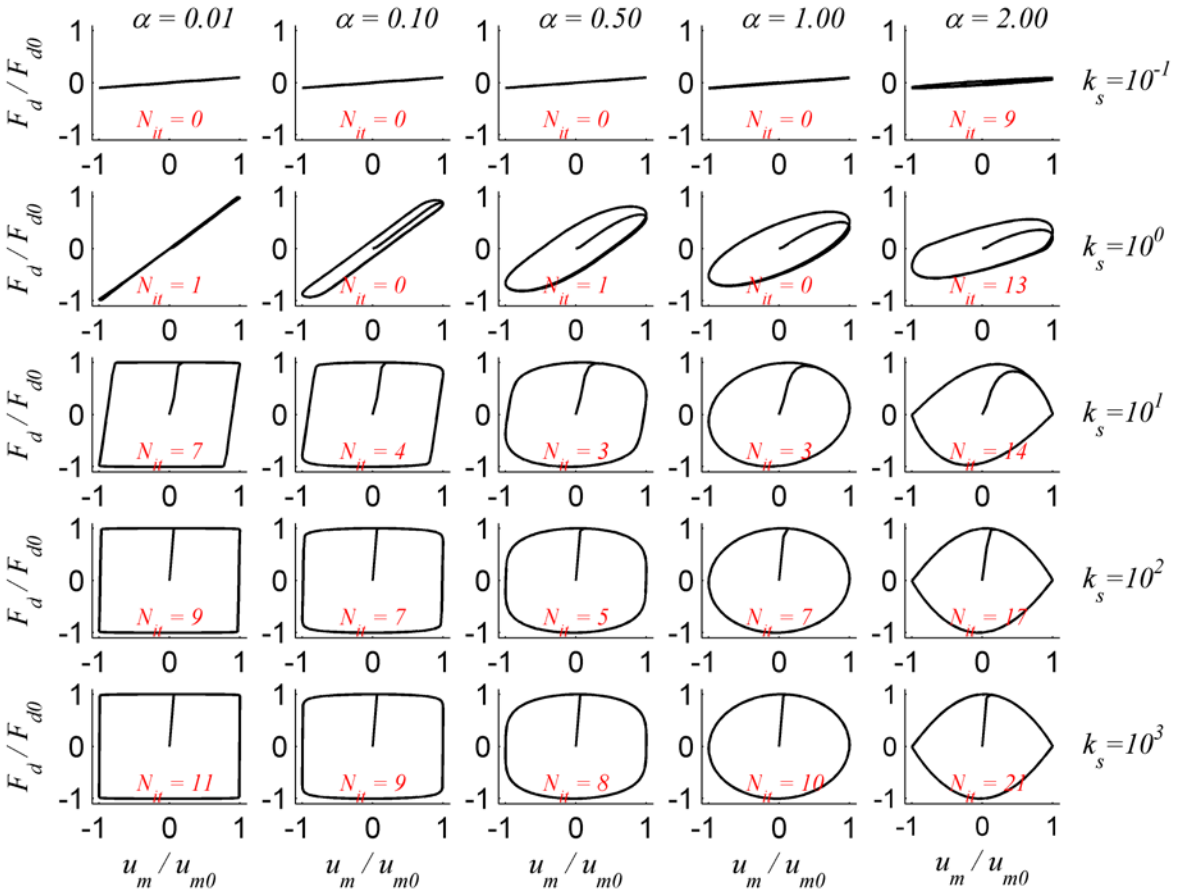

747

748

749 **Figure 5:** Force-displacement relations for nonlinear viscous dampers under sinusoidal displacement

750 loading based on the adaptive DP54 iterative method

751

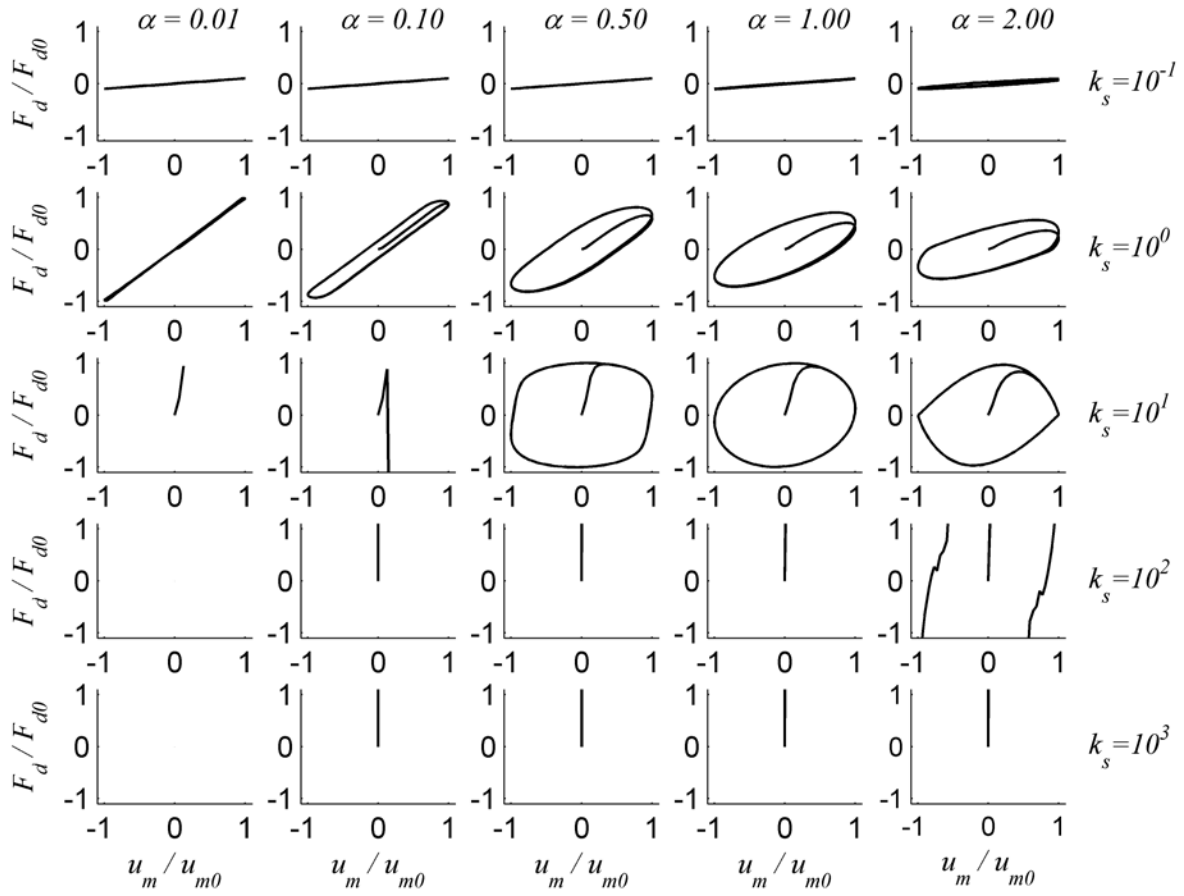

752

753

754 **Figure 6:** Force-displacement relations for nonlinear viscous dampers under sinusoidal displacement

755 based on the classical 4th order Runge-Kutta method

756

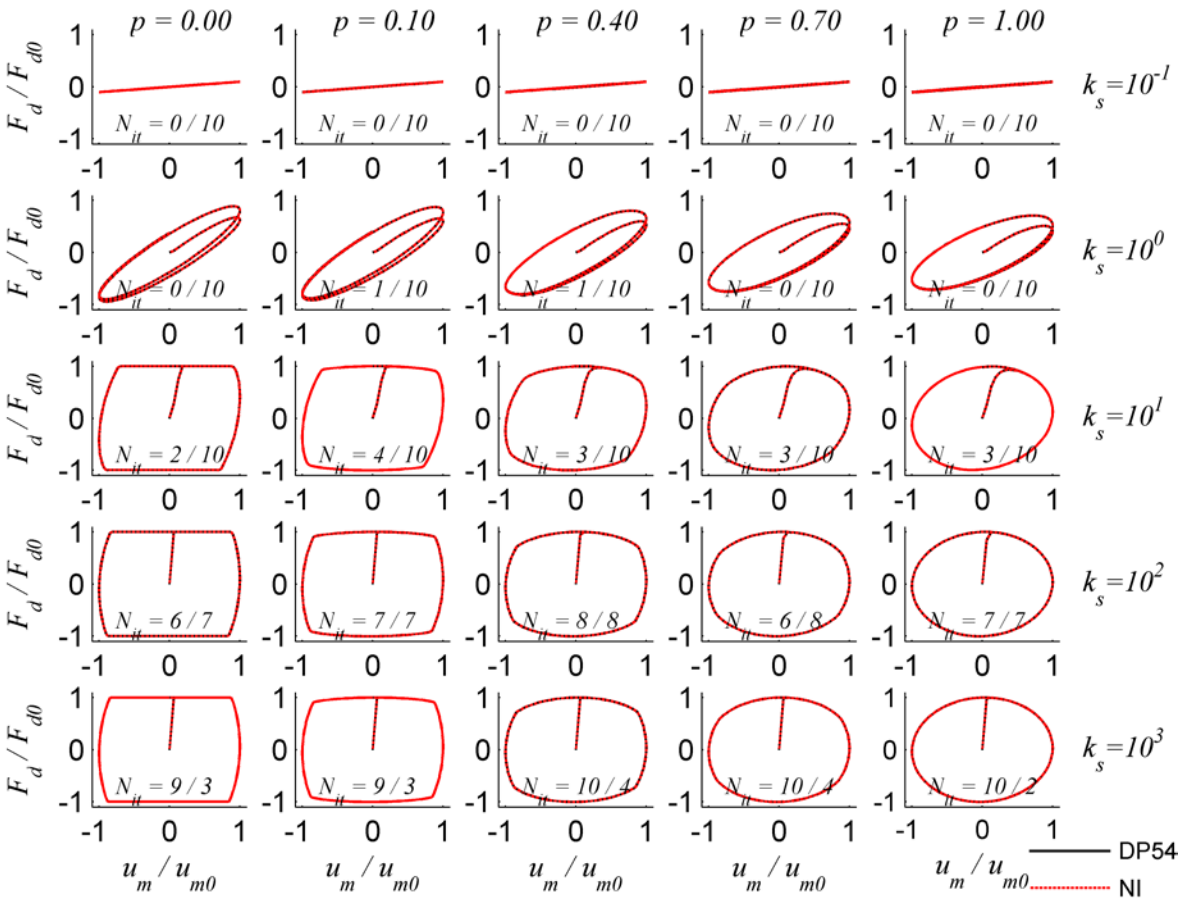

Figure 7: Comparison of the force-displacement relation predictions for bilinear oil dampers under sinusoidal displacement based on the adaptive DP54 iterative method and the alternative adaptive numerical integration algorithm (NI) for μ_m=2

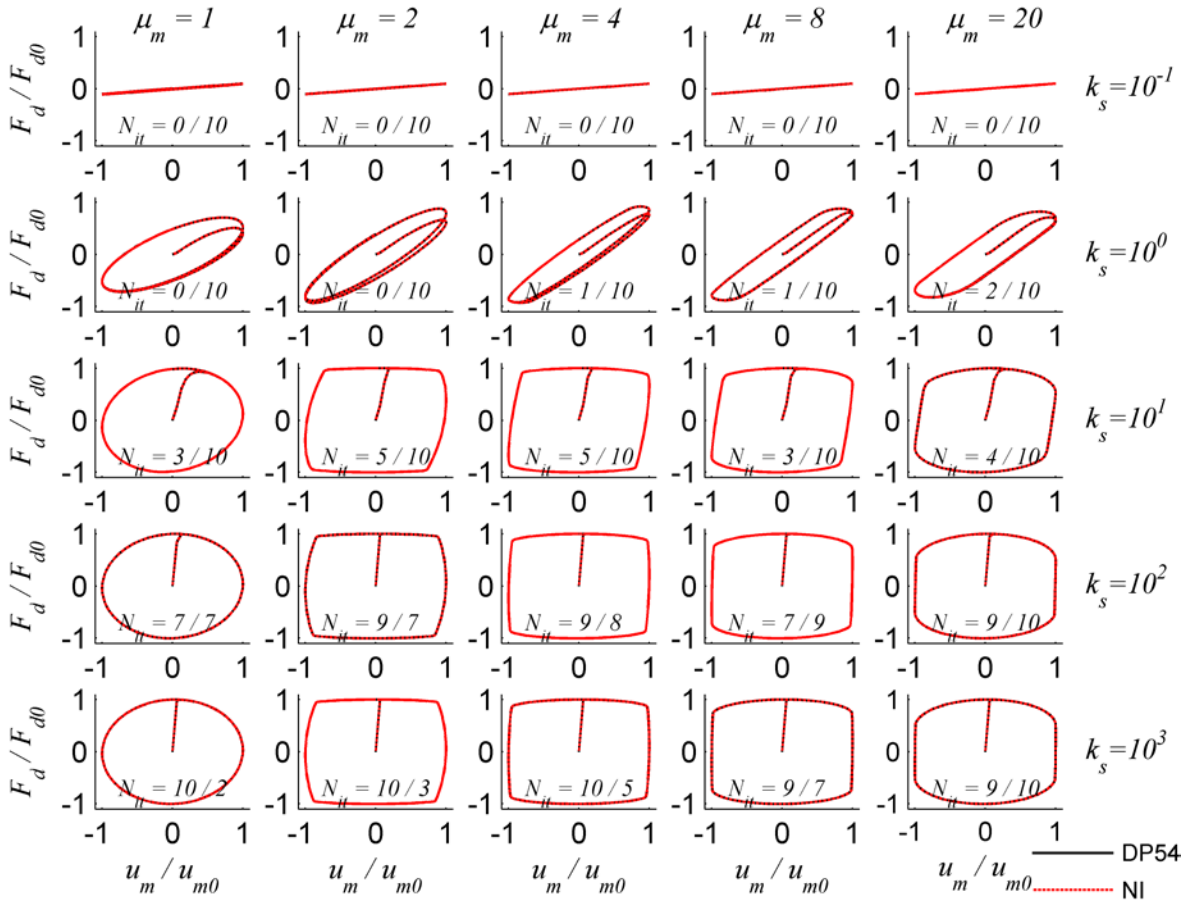

762

763

764 **Figure 8:** Force-displacement relations for bilinear oil dampers under sinusoidal displacement based on

765 the adaptive DP54 iterative method and the alternative adaptive numerical integration algorithm (NI) for

766 p=0.05

767

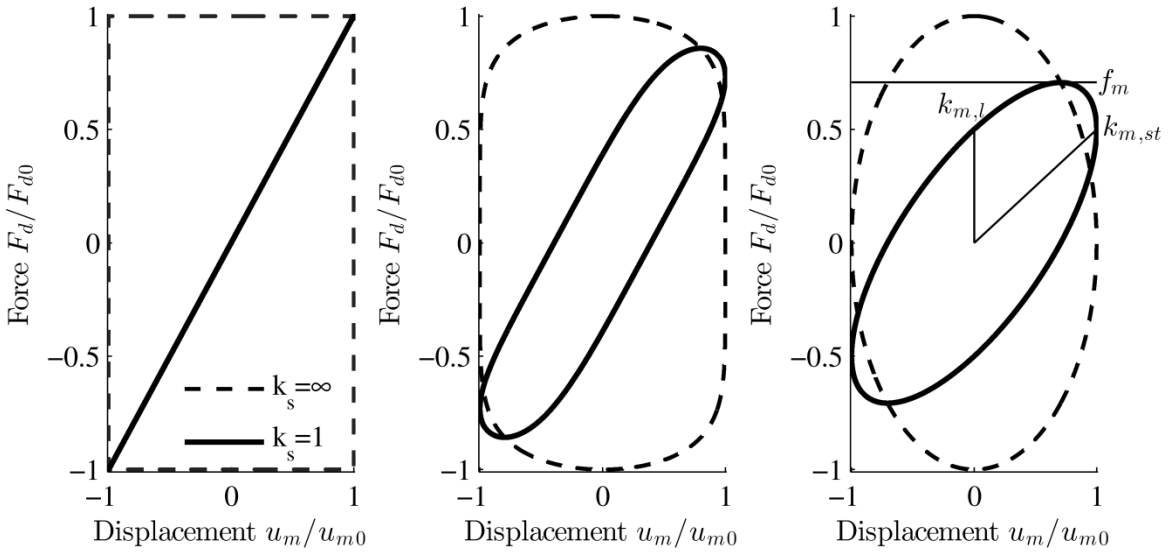

(a) α = 0 (b) α = 0.30 (c) α = 1.0

Figure 9: Variation of nonlinear viscous dampers force-displacement relations with different parameters under sinusoidal displacement and graphical definition of dynamic stiffness

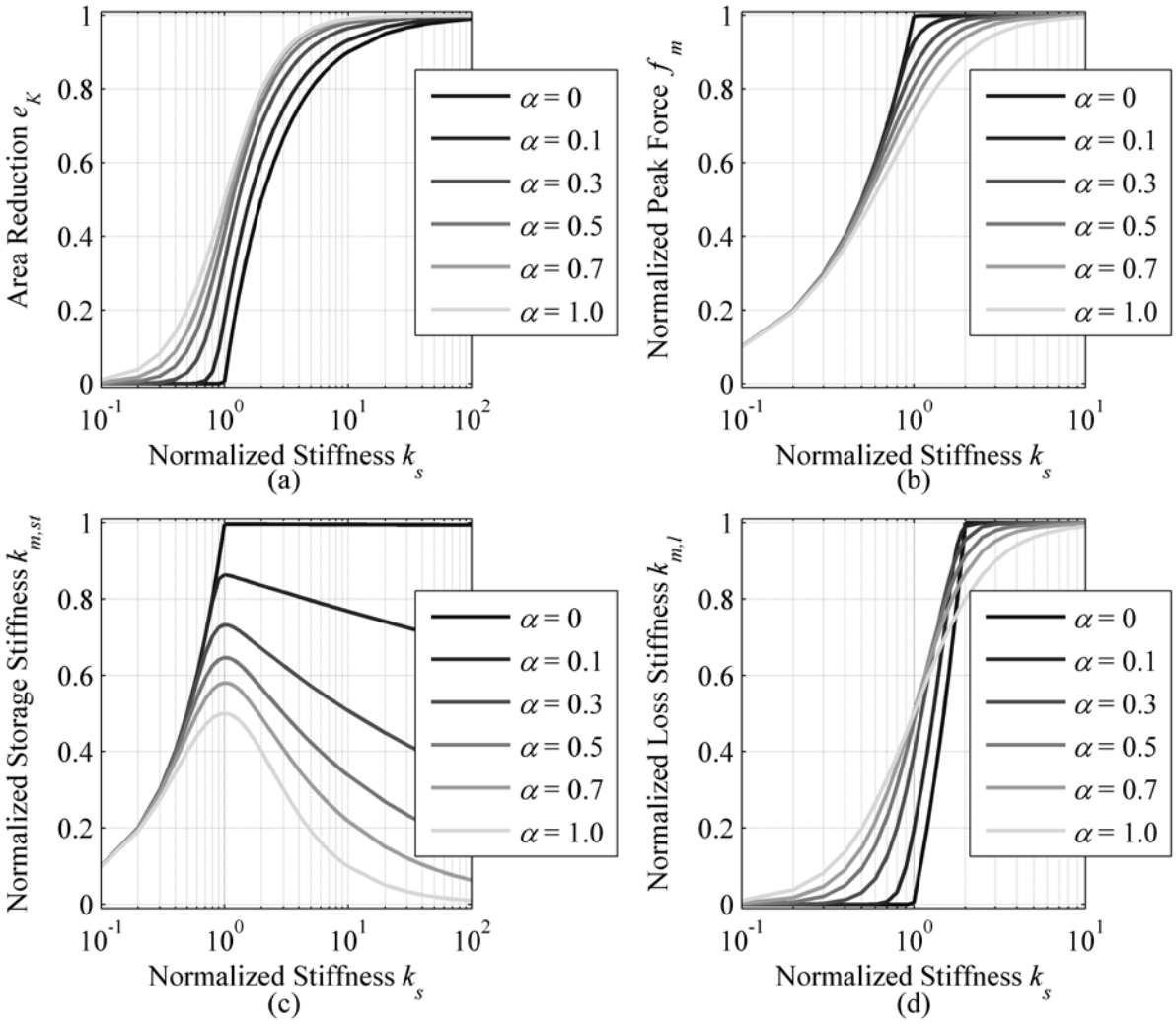

773

774

775 **Figure 10:** Effect of normalized stiffness on various properties of nonlinear viscous dampers with

776 different velocity exponents

777

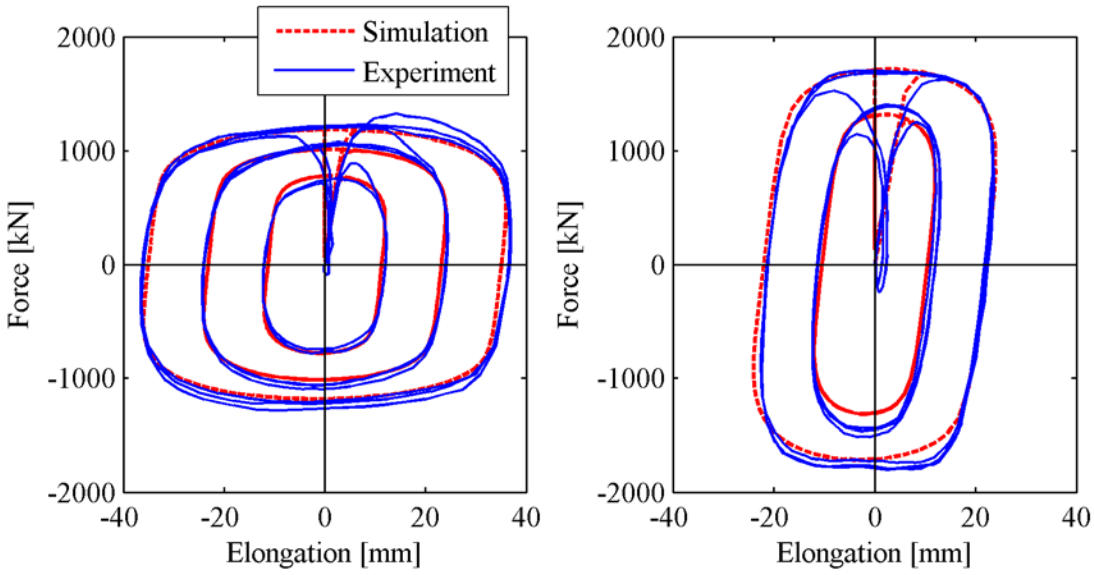

(a) 0.5 Hz (b) 2 Hz

Figure 11: Comparison of the simulated and experimental hysteretic response of nonlinear viscous dampers under dynamic sinusoidal loading (experimental data adopted from Kasai et al. 2004b)

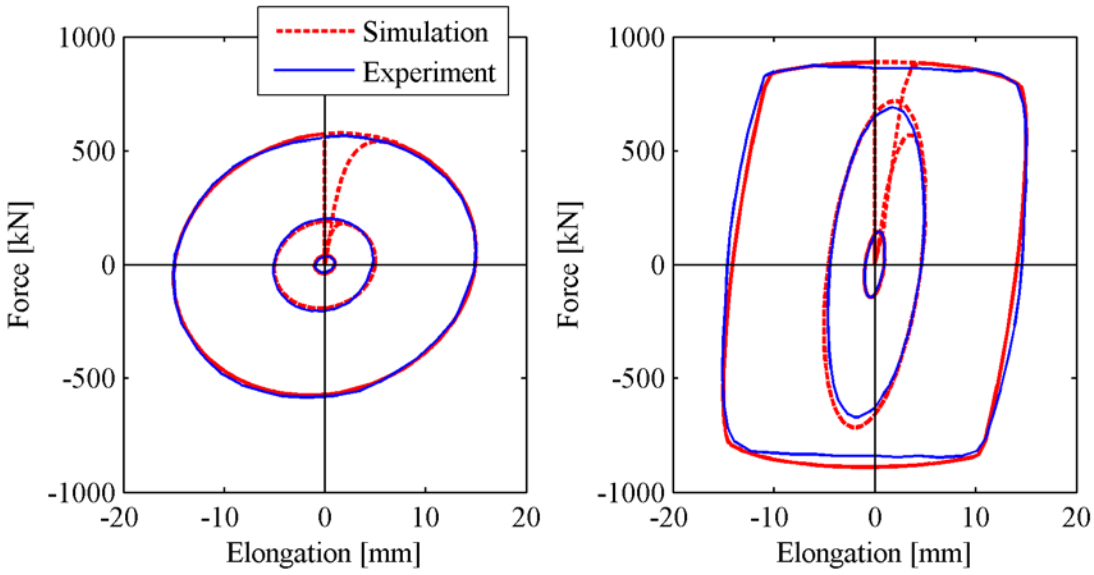

(a) 0.25 Hz (b) 1 Hz

Figure 12: Comparison of the simulated and experimental hysteretic response of bilinear oil dampers under dynamic sinusoidal loading (experimental data adopted from Kasai et al. (2004b)

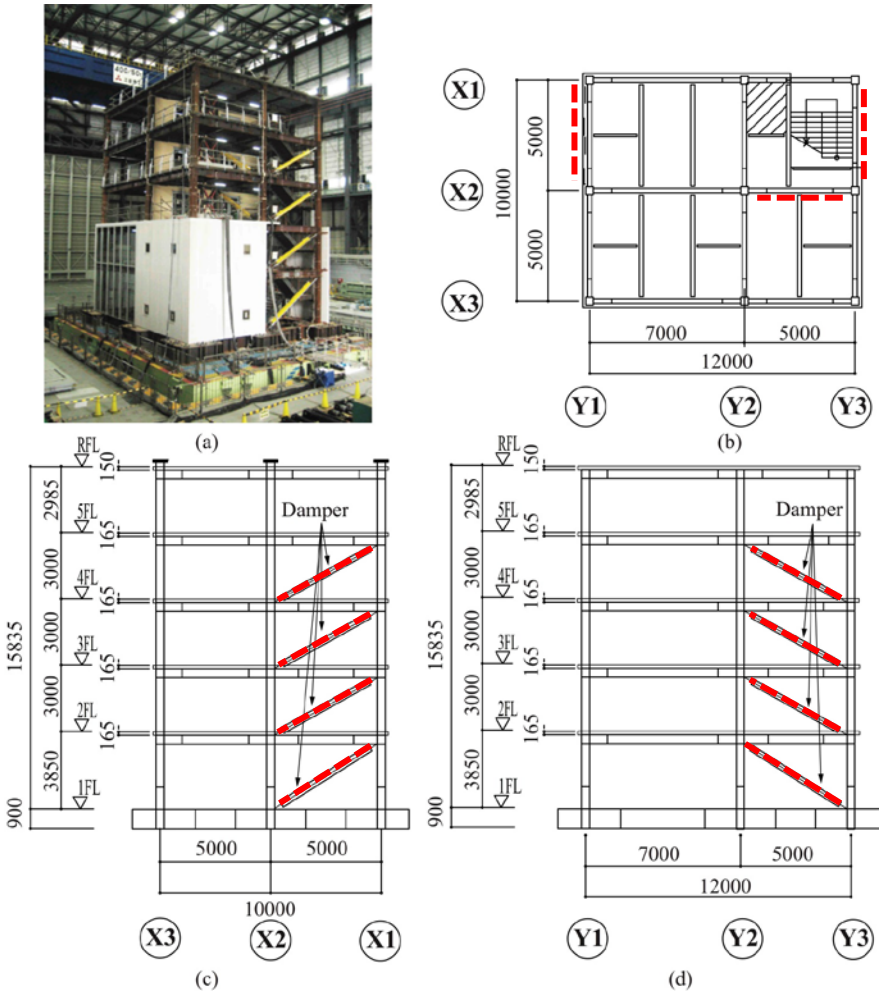

Figure 13: 5-story test-structure tested at E-Defense; (a) building after installation on the shake table; (b) plan view (c) elevation view in X- loading direction; (d) elevation view in Y-loading direction (images adopted from Akcelyan et al. (2016), dimensions in mm)

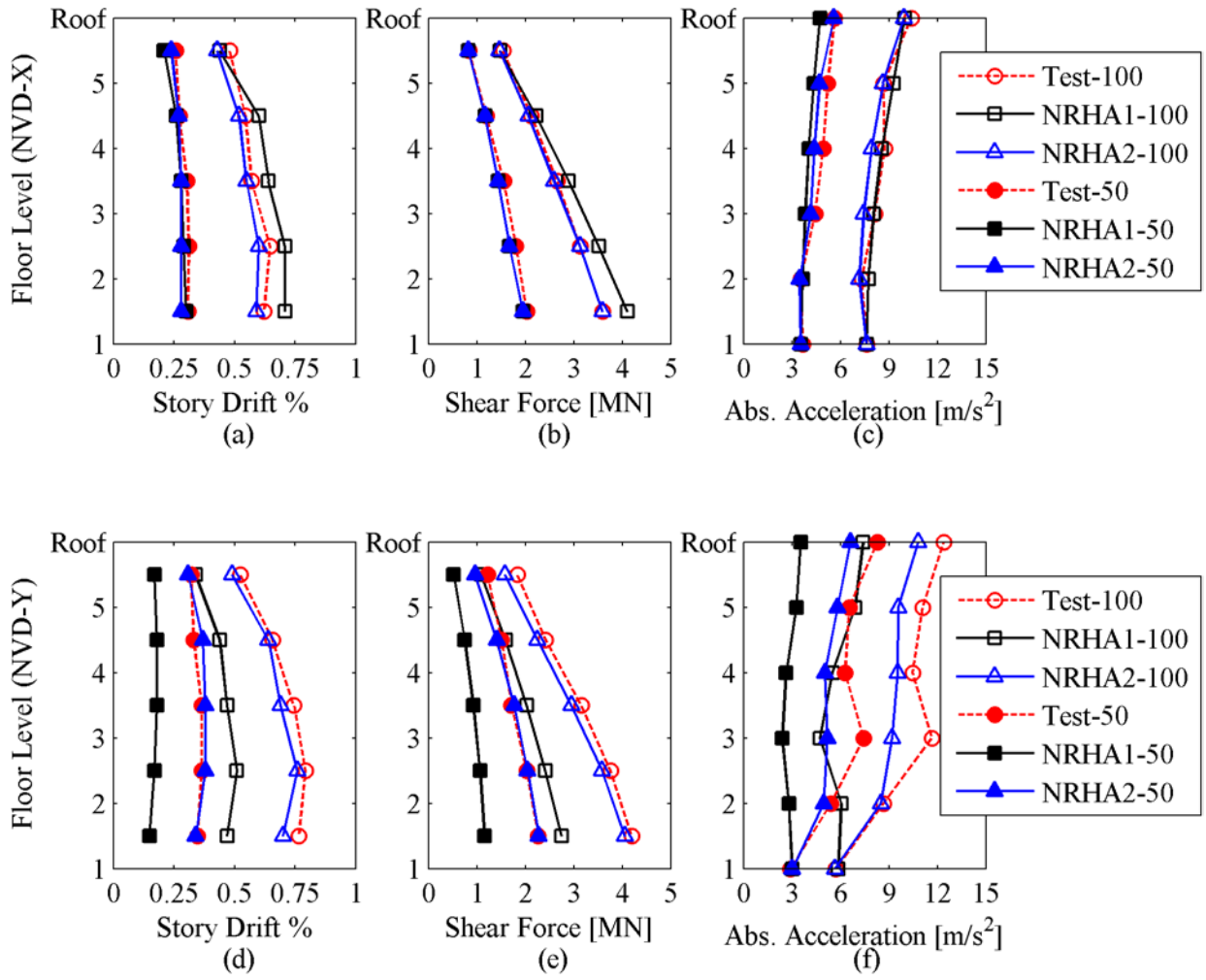

Figure 14: Comparison of computed and measured peak engineering demand parameters of the test structure with nonlinear viscous dampers (50% and 100% JR Takatori record)

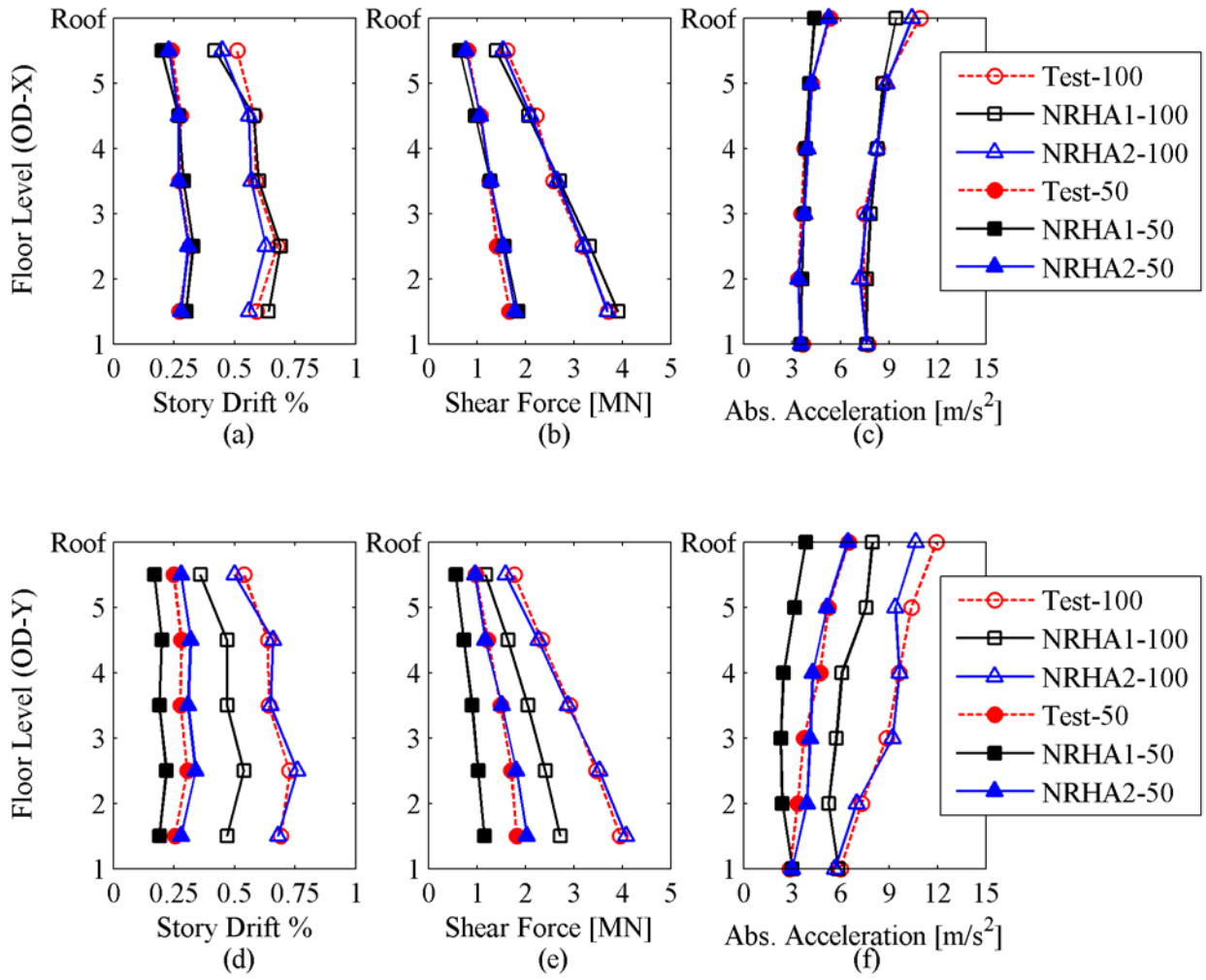

Figure 15: Comparison of computed and measured peak engineering demand parameters of the test structure with bilinear oil dampers (50% and 100% JR Takatori record)

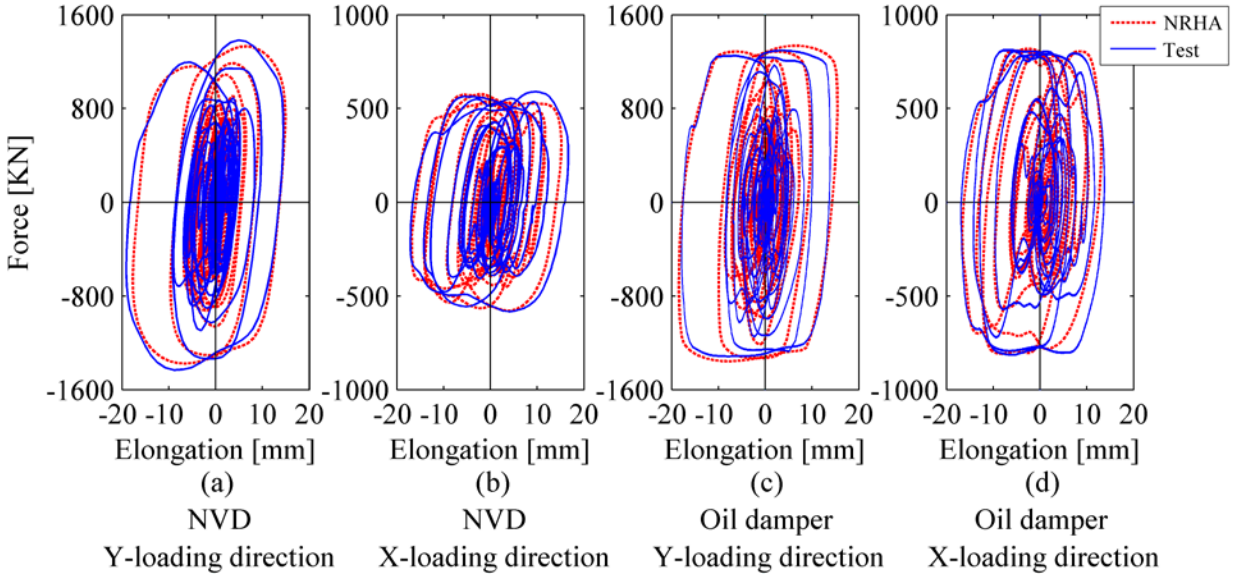

803

804 **Figure 16:** Comparison between the simulated and measured hysteretic response of nonlinear viscous and

805 bilinear oil dampers installed in the first story of the test structure (100% JR Takatori record)

806